MODELLING DIRECTION SOLIDIFICATION

NAG8-541

First Semi-annual Progress Report

1 September 1985 to 28 February 1986

CLARKSON UNIVERSITY

Potsdam, New York 13676

Principal Investigator: Dr. William R. Wilcox
Professor and Chair
Department of Chemical Engineering
315-268-6650

Graduate Student Research Assistants:

Mr. Greg Neugebauer, M.S. Candidate in Chemical Engineering

Ms. Lorraine Ruggiano, Ph.D. Candidate in Chemical Engineering

(NASA-CR-176606) MODELLING DIRECTION SOLIDIFICATION Semiannual Progress Report, 1 Sep. 1985 - 28 Feb. 1986 (Clarkson Univ.) 74 p HC A04/MF A01 CSCL 11F

N86-20543

Unclas
G3/26 05666

OBJECTIVE

This grant is a continuation of Contract NAS8-34891. The overall objective of this program is to develop an improved understanding of some phenomena of importance to directional solidification, to enable us to explain and predict differences in behavior between solidification on earth and solidification in space.

RESEARCH COMPLETED

The first six months of the new grant were devoted primarily to completion of research begun under the previous contract. One paper was published, three others were accepted for publication, two others were completed and submitted for publication, and an M.S. thesis completed. These are listed below.

1. "Thermal fields in the Bridgman-Stockbarger technique," H. Potts and W.R. Wilcox, J. Crystal Growth 73, 350 (1985).
2. "Chaotic asymmetric convection in the Bridgman-Stockbarger technique," H. Potts and W.R. Wilcox, J. Crystal Growth (in press).
3. "Behavior of a non-wetting melt in free fall: experimental," R. Sen Jayaraj and W.R. Wilcox, J. Crystal Growth (in press).
4. "Behavior of a non-wetting melt in free fall: theoretical," R. Sen Jayaraj and W.R. Wilcox, J. Crystal Growth (submitted).
5. "Twinning of dodecanedicarboxylic acid," R. Sen Jayaraj and W.R. Wilcox, J. Crystal Growth (in press).
6. "Validity of the Burton-Prim-Slichter equation," W.R. Wilcox, J. Crystal Growth (submitted)
7. "Influence of heater configuration on convection in the Bridgman-Stockbarger technique," G. Neugebauer, M.S. thesis.

All but one of these papers and the M.S. thesis are included as appendices in the final report of the previous contract, a draft of which was recently submitted to NASA MSFC. To avoid duplication, only the remaining paper (number 6) is attached here. During the last six months revisions were made in papers 2, 3 and 5. Papers 4 and 6 were written during this period, along with additional computations and preparation of additional figures for these papers.

RESEARCH INITIATED

Ms. Lorraine Ruggiano spent the last six months preparing for her qualifying examination, which consisted of surveying the literature and preparing a written research proposition, or proposal. She has chosen to study the influence of convection on the perfection of indium gallium antimonide. (In a Skylab experiment directed by Wilcox it was found that processing in space causes significant differences in the resultant ingots. Some differences were not immediately apparent and so did not appear in the Skylab proceedings, but only later in the Materials Research Bulletin.) Note that indium gallium antimonide is representative of the class of III-V, II-VI and other solid solution semiconductors which are of such great importance for infrared sensors, opto-electronics, quantum well devices, solar cells, etc. Examples include lead tin telluride and mercury cadmium telluride. Growth on earth with natural convection yields polycrystalline ingots with twins and unacceptable concentration variations. The causes of the twinning and polycrystallinity are not known. Some of the sources of concentration variation are known, but the influence of natural convection remains somewhat uncertain.

RESEARCH PLANS

Ms. Ruggiano will take her Ph.D. qualifying examination. She will construct the apparatus required for her experiments. She will purchase a rotating/pulling head, heating wires, ceramic components, silica tubing, high purity materials, etc. Ampoules will be prepared and slowly solidified with spin-up/spin-down (accelerated crucible rotation). The solidification will be perturbed to reveal the solid-liquid interface shape. The twin and grain structure will be compared in ingots grown with and without stirring.

In the next six months Mr. Neugebauer will defend his M.S. thesis, prepare his research proposition and take his Ph.D. qualifying examination. At the moment it appears that he will propose to use a transparent organic material to study the relationship between the temperature distribution in the heater, the natural convection currents, and the impurity distribution in crystals solidified from the melt. This represents an extension of his M.S. thesis in which he showed that axisymmetric convection is very difficult to obtain in the Bridgman-Stockbarger technique and that this convection can be controlled by varying the vertical and azimuthal variation in heater temperature. (It was even possible to reduce convection near the freezing interface to near zero by increasing the heater temperature with height.)

A paper on behavior of a melt in a non-wetted ampoule (numbers 3 and 4 above) will be presented at the Metallurgical Society meeting in New Orleans in March, at a microgravity session. Mr. Neugebauer will present an after dinner talk on his research to a local section of the American Association for Crystal Growth in New Jersey in March. At July's International Conference on Crystal Growth in York, England, 3 papers will be presented: "Validity of the Burton-Prim-Slichter Equation," "Convection in the Bridgman-Stockbarger Technique," and "Liquid Behavior in a Non-Wetted Ampoule."

VALIDITY OF THE BURTON-PRIM-SLICHTER EQUATION

William R. WILCOX
Department of Chemical Engineering and Center for Advanced Materials Processing, Clarkson University, Potsdam, New York 13676, USA

ABSTRACT

The following must be assumed in order to derive the classic Burton-Prim-Slichter equation for segregation during crystal growth: isobaric, isothermal, isopotential or uncharged species, binary, planar interface, steady state, constant diffusion coefficient in fluid, no diffusion in crystal, no lateral convection within fluid film at interface with complete mixing beyond (stagnant film model), and either density, total concentration or partial molar volumes constant in the fluid phase. In addition, the effective distribution coefficient and the interfacial distribution coefficient must be defined properly. The velocity in the equation is the growth rate times a factor correcting for the difference in volumetric properties between crystal and fluid. The stagnant film thickness δ is usually a function of growth rate, with the precise functionality depending on the type of convection occurring in the growth fluid. In general δ varies much more with laminar forced convection than with free convection or turbulent forced convection. The Wilson film thickness always varies much more strongly with growth rate than does the stagnant film thickness.

The results are also applicable to computation of growth and dissolution rates from solutions and gases.

1. Introduction

For many years the Burton-Prim-Slichter equation has provided the basis for interpreting experimental segregation data and for predicting the influence of stirring and finite freezing rate on the effective distribution coefficient k_{eff} [1]. However, many assumptions were made implicitly in its derivation. In order to make these assumptions clear, we rederive here the BPS equation from the most general assumption-free mass transfer equations.

In using the BPS equation it has generally been assumed that the stagnant film thickness δ is independent of freezing rate v_c. In the second part of this paper we use results from the hydrodynamic literature to show that δ can be a strong function of v_c at even moderate freezing rates.

2. Derivation of BPS Equation

In order to make clear all of the assumptions involved in BPS, we start its derivation with the general multicomponent diffusion equations of Reference [2]. The notation is the same as in Reference [2], and is also given here at the end. The subscripts denote first the component (i for multicomponent, A and B for binary), and second the phase (c for crystal, f for fluid (either liquid or gas), 0 for interfacial fluid, and ∞ for bulk fluid far from the interface). The superscript r denotes that a standard reference system is used, mole centered (m), mass centered (') or volume centered (v). These represent the choices of average fluid velocity that may be used. A choice is necessary because each component moves at a different velocity v_i in a fluid with mass transfer taking place. The diffusion equations are written in terms of the general parameters Z_i^r, α_{ij}^r and Y_i^r, which can take the values shown in Table 1.

TABLE 1

Diffusion Parameters in Different Reference Systems

Reference System	Z_i^r	α_{ij}^r	Y_i^r	Average Velocity	$\Sigma Z_i^r C_i$
Mass centered	M_i	ρ	W_i/M_i	$v' = \Sigma W_i v_i$	ρ
	M_i	$C^2 M_i M_j/\rho$	X_i/M_i		
(const. ρ)	M_i	1	$C_i = \rho_i/M_i$		
Mole centered	1	C	X_i	$v^m = \Sigma X_i v_i$	C
	1	ρ^2/CM_iM_j	W_i		
(const. C)	1	1	$C_i = CX_i$		
Volume centered	$\bar{V}_i$	1	C_i	$v^v = \Sigma F_i v_i$	1
(const. $\bar{V}_i$)	$\bar{V}_i$	$C^2\bar{V}_j\bar{V}_i$	$X_i/\bar{V}_i$		
(const. $\bar{V}_i$)	$\bar{V}_i$	$\rho^2\bar{V}_i\bar{V}_j/M_iM_j$	$W_i/\bar{V}_i$		

In the absence of chemical reactions, the multicomponent mass transfer equation is given by [2]:

$$\nabla \cdot J_{if}^r + \nabla \cdot C_{if} v_f^r = -\partial C_{if}/\partial t \tag{1}$$

The most common phenomenological expression used for the diffusion flux J_{if}^r in an isobaric, isothermal, isopotential (or non-electrolyte) system is:

$$J_i^r = -\sum_{j=1}^{n-1} \alpha_{ij}^r D_{ij}^r \nabla Y_j^r \tag{2}$$

Note that the flux of component i depends not only on its own concentration gradient Y_i but on the gradients of the other constituents as well.

To derive BPS, Equation (1) must be greatly simplified via the following:

(a) Binary, with $J_A^r = -\alpha_{AB}^r D_{AB} \nabla Y_A^i$. Note that D_{AB} is independent of reference system, whereas D_{ij}^r is not.

(b) One dimensional problem, so $\nabla = \partial/\partial y$. This is true only if the interface is planar and if there is no convection parallel to the interface (no stirring).

(c) D_{AB} is constant, enabling us to move D_{AB} out of the differential.

(d) Steady state, so $\partial C_{Af}/\partial t = 0$.

(e) $\Sigma Z^r_{if} C_{if}$ and Z^r_{if} are constant. This causes $\nabla \cdot v^r_f = 0$, thereby eliminating the $C_{Af} \nabla \cdot v^r_f$ term.

Note that the conditions in (e) correspond to constant density ρ_f for the mass centered system, constant total concentration C_f for the mole centered system, and constant partial molar volumes $\overline{V}_{Af}$ and $\overline{V}_{Bf}$ for the volume centered system. A constant density is approximated by some organic mixtures and by very dilute systems ($C_{AF} \ll C_f$). Constant C_f is found for ideal gas mixtures, while constant $\overline{V}_{Af}$ is fairly good for most liquid and gas mixtures. Thus the volume-centered system is the one of most general applicability. However, as pointed out later the average velocity appearing in the hydrodynamic equations is the mass-average velocity v'.

With assumptions (a) through (e), Equation 1 becomes:

$$D_{AB} \frac{\partial^2 C_{Af}}{\partial y^2} - v^r_f \frac{\partial C_{Af}}{\partial y} = 0 \qquad (3)$$

At this point we don't yet know what is the fluid velocity v^r_f. The condition $\nabla \cdot v^r_f = 0$ and absence of lateral convection insure that it is constant. (If $\Sigma Z^r_{if} C_i$ and Z^r_{if} are <u>not</u> both constant, v^r_f is likewise not constant.) Intuitively one feels that v^r_f must be related to the crystal growth rate v_c. The relationship is found by a material balance at the freezing interface, taking the interface to be fixed at y = 0 and assuming no diffusion in the solid [2,3]:

$$v_f^r = v_f^r(0) = -v_{cf} = -v_c \frac{Z_{Af}^r C_{AC} + Z_{Bf}^r C_{BC}}{Z_{Af}^r C_{Af} + Z_{Bf}^r C_{Bf}} \tag{4}$$

The negative sign comes from the fact that v_f^r is directed out of the interface into the fluid (positive y), while v_{cf} and v_c are traditionally taken to be in the opposite direction. Equation (4) gives $(v_{cf}/v_c) = \rho_c/\rho_f$ for the mass-centered system, C_c/C_f for the mole centered system, and $\overline{V}_{Af}C_{AC} + \overline{V}_{Bf}C_{BC}$ for the volume centered system. For $C_{Af} \ll C_f$, all are equivalent.

To solve Equation (3) with $v_f^r = -v_{cf}^r$ we need the boundary conditions:

$$\left.\begin{aligned} &\text{at } y = 0 \text{ (interface):} && C_{Af} = C_{A0} \\ &\text{at } y = \delta^r: && C_{Af} = C_{A\infty} \end{aligned}\right\} \tag{5}$$

Note that this is equivalent to assuming the stagnant film model, in which it is imagined that there is no lateral convection within a layer of thickness δ at the freezing interface, with complete mixing beyond this giving a uniform concentration $C_{A\infty}$. Note that the value of δ depends on the reference system. The solution of Equations (3) and (5) is

$$\frac{C_{Af} - C_{A0}}{C_{A\infty} - C_{A0}} = \frac{1 - \exp(-y v_{cf}^r / D_{AB})}{1 - \exp(-\delta^r v_{cf}^r / D_{AB})} \tag{6}$$

To obtain the BPS equation we need a material balance for the impurity A across the interface. Assuming no diffusion in the solid this is, at y = 0:

$$v_c C_{AC} = D_{AB} \frac{\partial C_{Af}}{\partial y} + C_{A0} v_{cf}^r \tag{7}$$

If we differentiate Equation (6) and substitute into Equation (7) we get the BPS equation only if we define the distribution coefficients as follows:

$$k_0^r = \frac{C_{AC}}{C_{A0}(v_{cf}^r/v_c)} \quad ; \quad k_{eff}^r = \frac{C_{AC}}{C_{A\infty}(v_{cf}^r/v_c)} \tag{8}$$

The correct form of BPS is thereby:

$$k^r_{eff} = \frac{k^r_0}{k^r_0 + (1-k^r_0)\exp[-\delta^r v_c (v^r_{cf}/v_c)/D_{AB}]} \qquad (9)$$

Note that k^r_0 is not the equilibrium distribution coefficient, but is the interfacial distribution coefficient. While these distribution coefficients may be identical at low freezing rates, they certainly are not equal at high freezing rates. It is also worth noting that Eqs. (8) actually correspond to common usage, because concentrations have been based on analyses of solids rather than on concentrations in the liquid at the melting point. Since the liquid has a density different from that of the solid, when one melts a solid the impurity concentration (in atoms/volume) changes.

3. Variation of Stagnant Film Thickness

There is no such thing as a stagnant film in convective mass transfer, even if it is erroneously called by the sophisticated sounding name ''boundary layer.'' In actuality the lateral velocity parallel to a solid surface (such as a freezing interface) only approaches zero as one approaches the surface. In mass transfer problems, the fictitious film thickness δ is defined as that giving the correct answer. In that sense, within the validity of the other assumptions made, the BPS equation is correct because δ is defined as having that value required to make it correct. In practice, therefore, δ must be obtained from experiments, from solutions of the real boundary-layer equations, or solutions of the exact hydrodynamic and mass transfer equations. It turns out that δ is a function of D_{AB}, the kinematic viscosity ν, and the freezing rate v_c.

In correlating segregation data, a convenient technique is to rearrange BPS into the form:

$$\left(\frac{1}{k^r_{eff}} - 1\right) = \left(\frac{1}{k^r_0} - 1\right) \exp\left(-\frac{\delta^r v_c (v^r_{cf}/v_c)}{D_{AB}}\right) \tag{10}$$

so that one plots experimental values of $\ln(1/k^r_{eff}-1)$ vs. growth rate v_c to obtain δ from the slope and k_o from the intercept. However, this is an accurate procedure <u>only</u> if δ^r is not a function of v_c.

In predicting segregation from theory, values of δ are by far most available for $v_c = 0$. (We denote these as δ^*.) But does $\delta = \delta^* =$ constant? We can answer this for only some mass transfer situations, using experimental data and theoretical results in the existing literature. Most of the results are actually for heat transfer, requiring substitution of Sherwood number Sh for Nusselt number Nu, concentration gradient for temperature gradient, and Schmidt number Sc for Prandtl number Pr.

The methods used to convert the literature results to a form useful and familiar to us were outlined in Reference [4] and are based on Equations (6) and (7). The equations used are:

$$\frac{\delta^r}{\delta^*} = \frac{\ln(1 + \varepsilon^r_v)}{\varepsilon^r_v (Sh/Sh^*)} \tag{11}$$

$$\frac{\delta^* v^r_{cf}}{D_{AB}} = -\varepsilon_v \frac{Sh}{Sh^*} \tag{12}$$

where the interfacial velocity parameter ε^r_v is defined as

$$\varepsilon^r_v = \frac{C_{A\infty} - C_{A0}}{C_{AC}/(v^r_{cf}/v_c) - C_{A0}} \tag{13}$$

and

$$\delta^r v^r_{cf}/D_{AB} = -\ln(1 + \varepsilon^r_v) \tag{14}$$

Note that for constant ρ_f in the mass-centered system, $\varepsilon_v' = (W_{A\infty}-W_{A0})/W_{Ac}-W_{A0})$ while for constant C_f, $\varepsilon_v^m = (X_{A\infty}-X_{A0})/(X_{Ac}-X_{A0})$. The negative of ε_v is the same as Δ used by Wilson [5], which she equated to $\delta_w v_c/D$. Here we have used the subscript w to denote the Wilson film thickness. This would be the stagnant film thickness if the concentration profile were linear in the film. However as we see in Eq. (6), the fluid flow feeding the crystal growth would cause the concentration profile to be exponential in a stagnant film. That is, if we had a real stagnant film, δ and δ_w both would equal δ^* at very low growth rates, both only δ would remain constant as v_c is increased. We now see that exact theories predict that both δ and δ_w vary with v_c, but δ_w more so than δ. Thus one is most likely to obtain correct results by using δ.

Before discussing the literature results, we note that δ is also useful in calculating growth rates and dissolution rates for solutions and vapors. The concentration in the equations now refers to solute concentration rather than impurity concentration.

a. Rotating disk

Figure 1 shows results for laminar flow caused by an infinite rotating disk. The theoretical curves are the same as those presented in 1969 [4]. For gases (Sc=1), δ is independent of v_{cf}. For liquids (high Sc), the ''exact'' results of Burton, Prim and Slichter [1], the results of the hydrodynamicists [5,6], and the results of Wilson [5] all agree. The others considered an infinite body of liquid, while Wilson used an infinite non-rotating plane parallel to the rotating disk. Consequently Wilson's δ^* values are about 15% larger than obtained by the others. That is, the non-rotating parallel surface reduced the mass transfer. In addition, Wilson summarized her results in a simple equation, which becomes in the present notation:

$$\frac{\delta'}{\delta^*} = \frac{1}{1 + 0.0699\ \delta' v'_{cf}/D_{AB}} \qquad (15)$$

Also shown on Figure 1 are data for segregation of Sb in Czochralski growth of Ge, published as a companion article [8] to the BPS theoretical paper. The scatter is considerable. A statistical treatment of the data revealed the predicted dependence of δ' on rotation rate and no dependence of δ'/δ^* on freezing rate. That is, within experimental accuracy the data agree with the theory.

On the other hand, the data on dissolution of KBr and sucrose in water [9] do not agree with theory. This was attributed to variable properties. In such concentrated solutions, viscosity, density and diffusion coefficient are all functions of composition, while the simple theory assumes that all of these properties are constant.

It is of interest to determine the error caused by neglecting the freezing rate dependence of δ' in the BPS equation. From Equation (9),

$$\% \text{ error} = 100\% \left[\frac{k'_0 + (1-k'_0)\exp(-\delta' v'_{cf}/D_{AB})}{k'_0 + (1-k'_0)\exp(-\delta^* v'_{cf}/D_{AB})} - 1 \right] \qquad (16)$$

Figure 2 shows that for typical Czochralski growth rates ($\delta^* v_{cf}/D_{AB} \sim 1$), the error never exceeds 10%. Similarly for $0.2 \lesssim k_0$ the error is 10% or less at all freezing rates. However for $k_0 \leq 0.1$ and moderate freezing rates the error becomes sizeable, and increasingly so as k_0 decreases. At very large freezing rates the error again decreases. As v_{cf} increases the mass transfer becomes increasingly determined by diffusion and by the crystallization flow, and less and less by convective mixing; $k_{eff} \to 1$, corresponding to steady state in the absence of mixing.

The influence of a magnetic field on segregation with a rotating disk was calculated by Hurle and Series [10]. Figure 3 shows their results for $\eta \to 0$ converted to $(\delta v'_{cf}/D\eta)$ vs. θ, where $\eta = (v'_{cf}/D)\ (\nu/\omega)^{1/2} Sc^{-1/4}$ and θ is a magnetic interaction parameter. As expected, increasing the magnetic field increases δ. Figure 4 shows the change of δ with increasing growth rate vs. magnetic field. Note that δ becomes significantly more sensitive to growth rate as the magnetic field increases.

Figure 5 compares the variation in Wilson film thickness with the variation in stagnant film thickness, with and without a magnetic field. The variation in Wilson thickness is significantly larger, especially without a magnetic field applied. This is true for all available data for all types of convection.

b. Forced convection

Figure 6 shows theoretical results from several authors for laminar forced convection parallel to a flat plate [11-27]. The negative values of $\delta^* v'_{cf}/D$ correspond to melting or dissolution, or as the hydrodynamicists express it, blowing rather than suction. Note that for Sc=0.7 the variation in δ depends strongly on the boundary condition assumed at the surface of the crystal. Unlike the results for a rotating disk, δ varies much more for gases than for liquids (large Sc).

Generally theorists assume constant density and viscosity in the fluid, because this greatly simplifies their task. In practice, however, these properties vary, sometimes considerably. Figure 7 shows the effect of a 10 fold change in density in going from the crystal surface to the bulk fluid, for forced convection over a flat plate. For gases, a variation in density has no effect, while for liquids the effect is large. Thus in solidification with large segregation and large differences in density of the constituents, one might expect significant deviations from constant density results.

At high fluid velocities the flow becomes turbulent. Figure 8 shows results for air on a flat plate for v'_{cf} independent of length along the plate. Figure 9 shows results for a variety of other boundary conditions. Note that there is considerable scatter in the experimental data. For constant v'_{cf} along the plate it would seem reasonable to take δ as constant, while with v'_{cf} decreasing with distance down the plate δ seems to increase with increasing $\delta^* v'_{cf}/D$.

Figure 10 shows results for laminar flow around the front of a blunt object. While δ varies more with gases, the difference between gases and liquids in small, particularly for growth (suction). Figure 11 shows the correlation of numerical computations for laminar flow of gases around a sphere with uniform v'_{cf}. Note that δ does not vary strongly and reaches a minimum at about $\delta^* v'_{cf}/D = 0.6$.

c. Natural convection

Now we consider convection driven by buoyancy. While the results are for density changes caused entirely by variations in concentration, similar results are expected for situations in which the variations in density are driven predominantly by variations in temperature.

Figure 12 shows the theoretical results for free convection of gases on a vertical flat plate with different boundary conditions at the crystal surface. The wide variation in predicted behavior provides little guidance and one may conclude that one might as well assume δ' independent of v'_{cf}.

Figure 13 shows experimental and theoretical results for free convection of liquids over a vertical flat plate. The theoretical results predict little variation in δ' with v'_{cf}, while the experimental data for dissolution (blowing) show δ increasing as the amount of dissolution decreases. This is the reverse trend from those for forced convection.

Figure 14 shows theoretical results for free convection around the leading portion of bodies. For both gases and liquids little change in δ' is predicted for growth (suction).

Figure 15 shows that significantly different results are predicted for liquid metals when a portion of the density change in the fluid results for temperature variations.

NOMENCLATURE

C Total molar concentration ($= \Sigma C_i$) (mol/m^3).

C_i Molar concentration of component i (mol/m^3).

D^r_{ij} Multicomponent diffusion coefficient in reference system r (m^2/s).

D_{AB} Binary diffusion coefficient (m^2/s).

F_i Volume fraction of i ($=C_i V_i$).

J^r_i Diffusion flux relative to r-average velocity v^r ($= C_i(v_i - v^r)$) (mol/$m^2 \cdot s$).

K Mass transfer coefficient ($= DSh/L$) (m/s).

k Distribution coefficient (See Eq. 8).

L Characteristic dimension or length (m).

M_i Molecular weight of i (g/mol).

Pr Prandtl number (ν/κ).

Re Reynolds number, $U_\infty x/\nu$.

Sc Schmidt number (ν/D_{AB}).

Sh Sherwood number $((\partial(W_A - W_{A\infty})/W k_{A0} - W_{A\infty}))/\partial(y/L))$.

U_∞ Free stream velocity of fluid (m/s).

V_i Partial molar volume of i (m^3/mol).

v^r Average velocity in y direction in r reference system (m/s).

v_c Crystal growth velocity (m/s).

v_i Velocity in y direction of component i (m/s).

v^r_{cf} Crystallization flow velocity in negative y direction taking interface as fixed at y=0 (m/s). Same as V in figures.

W_i Weight fraction of i in mixture.

X_i Mole fraction of i.

x Distance along surface in flow direction (m).

Y^r_i Composition variable (see Table 1).

y Distance from interface into fluid (m).

Z^r_i Weighting factor (See Table 1).

α^r_{ij} Weighting factor (See Table 1).

Δ $\delta'_w v'_{cf}/D = -\varepsilon'_v$.

δ^r Fictitious stagnant film thickness (m).

ε^r_v Interfacial velocity parameter (See Eq. 13).

η $(v'_{cf}/D)(\nu/\omega)^{1/2} Sc^{-1/4}$.

κ Thermal diffusivity (m^2/s).

μ Viscosity (g/m s).

ν Kinematic viscosity ($= \mu/\rho$)(m^2/s).

ω Rotation rate (s^{-1}).

θ Magnetic interaction parameter [10].

ρ Total density (g/m^3).

Subscripts

A Solute in binary mixture.

B Solvent in binary.

c Crystal.

eff Effective value.

f Fluid (liquid or gas).

i Component i in multicomponent mixture.

j Component j.

0 Value at interface.

w Wilson value, based on linear concentration profile through film. (Ref. [5]).

∞ Value in bulk fluid.

Superscripts

m Mole centered (based on mole-average velocity).

v Volume centered (based on volume-average velocity).

' Mass centered (based on mass-centered velocity).

* Value for zero interfacial velocity ($v^r_{cf} = 0$, $v_c = 0$, $\varepsilon^r_v = 0$).

Acknowledgement

This work was supported by NASA via grants NAG 8-480 and NAG8-54. I am grateful to Professors Taylor and Subramanian for their encouragement.

REFERENCES

[1]. J. A. Burton, R. C. Prim and W. P. Slichter, J. Chem. Phys. 21 (1953) 1987.

[2]. W. R. Wilcox, Ch. 3 in Preparation and Properties of Solid State Materials, Vol. 2, Dekker, NY (1976).

[3]. W. R. Wilcox, J. Crystal Growth 12 (1972) 93.

[4]. W. R. Wilcox, Mat. Res. Bull. 4 (1969) 265.

[5]. L. O. Wilson, J. Crystal Growth 44 (1978) 371.

[6]. D. W. Zeh and W. N. Gill, AIChE Journal 14 (1968) 715.

[7]. D. R. Olander, J. Heat Transfer, Trans. ASME C84 (1962) 185.

[8]. J. A. Burton, E. D. Kolb, W. P. Slichter and J. D. Struthers, J. Chem. Phys. 21, (1953) 1991.

[9]. A. S. Emanuel and D. R. Olander, Int. J. Heat Mass Transfer 7 (1964) 539.

[10]. D. T. J. Hurle and R. W. Series, J. Crystal Growth 73 (1985) 1.

[11]. A. Acrivos, J. Fluid Mechanics 12 (1962) 337.

[12]. W. E. Stewart, AIChE J. 8 (1962) 421.

[13]. D. B. Spalding, W. M. Pun and S. W. Chi, Int. J. Heat Mass Transfer 3 (1962) 79.

[14]. H. J. Merk, Appl. Sci. Res. 8A (1959) 237.

[15]. W. E. Stewart, AIChE J. 9 (1963) 528.

[16]. O. T. Hanna, AIChE J. 11 (1965) 706.

[17]. H. L. Evans, Int. J. Heat Mass Transfer 3 (1961) 321.

[18]. W. E. Stewart and R. Prober, Int. J. Heat Mass Transfer 5 (1962) 1149.

[19]. H. S. Mickley, R. C. Ross, A. L. Squyers and W. E. Stewart, ''Heat, Mass, and Momentum Transfer for Flow over a Flat Plate with Blowing or Suction,'' NACA TN3208 (1954).

[20]. D. B. Spalding and H. L. Evans, Int. J. Heat Mass Transfer 2 (1961) 314.

[21]. A. Acrivos, AIChE J. 6 (1960) 410.

[22]. J. P. Hartnett and E. R. G. Eckert, Trans. ASME 79 (1957) 247.

[23]. D. B. Spalding and H. L. Evans, Int. J. Heat Mass Transfer 2 (1961) 314.

[24]. D. B. Spalding, Proc. Roy. Soc. 221A (1954) 100.

[25]. J. P. Hartnett and E. R. G. Eckert, p. 142 in ''Recent Advances in Heat Transfer,'' ed. J. P. Hartnett, McGraw-Hill, NY (1961).

[26]. T. S. Chen and E. M. Sparrow, J. Heat Transfer 98 (1976) 674.

[27]. E. M. Sparrow and J. B. Starr, Int. J. Heat Mass Transfer 9 (1966) 508.

[28]. E. Brundrett, W. B. Nicoll and A. B. Strong, J. Heat Transfer 94 (1972) 23.

[29]. R. H. Pletcher, J. Heat Transfer 96 (1974) 89.

[30]. K. Torii, N. Nishiwaki and M. Hirata, Proc. Third International Heat Transfer Conference, The Science Press, Inc. (1966).

[31]. T. Cebeci and G. J. Mosinskis, J. Heat Transfer 93 (1971) 271.

[32]. R. J. Moffat and W. M. Kays, Int. J. Heat Mass Transfer 11 (1968) 1547.

[33]. V. M. K. Sastri and J. P. Hartnett, FC8.6 in ''Heat Transfer,'' Vol. III, eds. U. Grigull and E. Hahne, Elsevier, Amsterdam (1970).

[34]. W. H. Thielbahr, W. M. Kays and R. J. Moffat, ''The Turbulent Boundary Layer on a Porous Plate. Experimental Heat Transfer with Uniform Blowing and Suction, with Moderately Strong Acceleration,'' Stanford University, Report HMT-11 (1970).

[35]. W. P. Manos and D. E. Taylor, Int. Dev. Heat Transfer, ASME, NY (1963) 731.

[36]. P. Chuchottaworm, A. Fujinami and K. Asano, J. Chem. Eng. Jap. 17 (1984) 1.

[37]. J. F. Clarke, J. Fluid Mech. 57 (1973) 45.

[38]. W. N. Gill, E. Del Casal and D. W. Zeh, Int. J. Heat Mass Transfer 8 (1965) 1135.

[39]. D. V. Cardner, Ph.D. Dissertation, Rice University, Houston (1963).

[40]. J. H. Merkin, Int. J. Heat Mass Transfer 15 (1972) 989.

[41]. R. Eichhorn, J. Heat Transfer 82 (1960) 260.

[42]. G. B. Lewis, J. L. Novotny and K. T. Yang, J. Heat Transfer 99 (1977) 446.

[43]. J. H. Merkin, Int. J. Heat Mass Transfer 18 (1975) 237.

[44]. W. E. Stewart, Int. J. Heat Mass Transfer 14 (1971) 1013.

[45]. D. V. Cardner and J. D. Hellums, I βEC Fund. 6 (1967) 376.

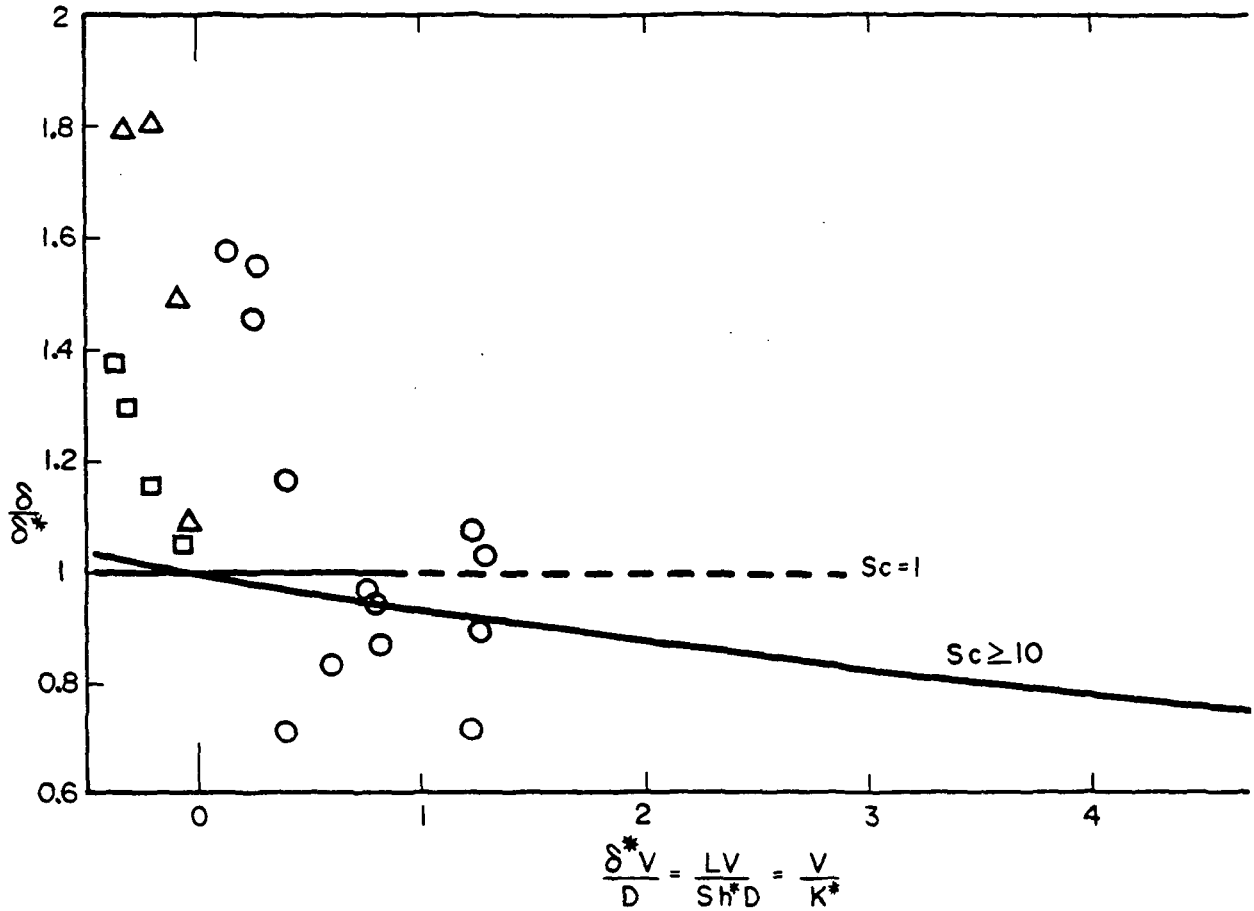

Figure 1. Laminar convection on an infinite rotating disk. Here $V = v'_{cf}$ is the crystallization flow in the mass centered system. Solid curves represent theoretical results of References [1,5-7] for liquids ($Sc \geq 10$) and of Reference [7] for gases ($Sc = 1$).

○ - Experimental data of Ref. [8] on segregation of Sb in Czochralski growth of Ge.

□ - Experimental data of Ref. [9] for dissolution of KBr in water.

△ - Sucrose dissolution in water [9].

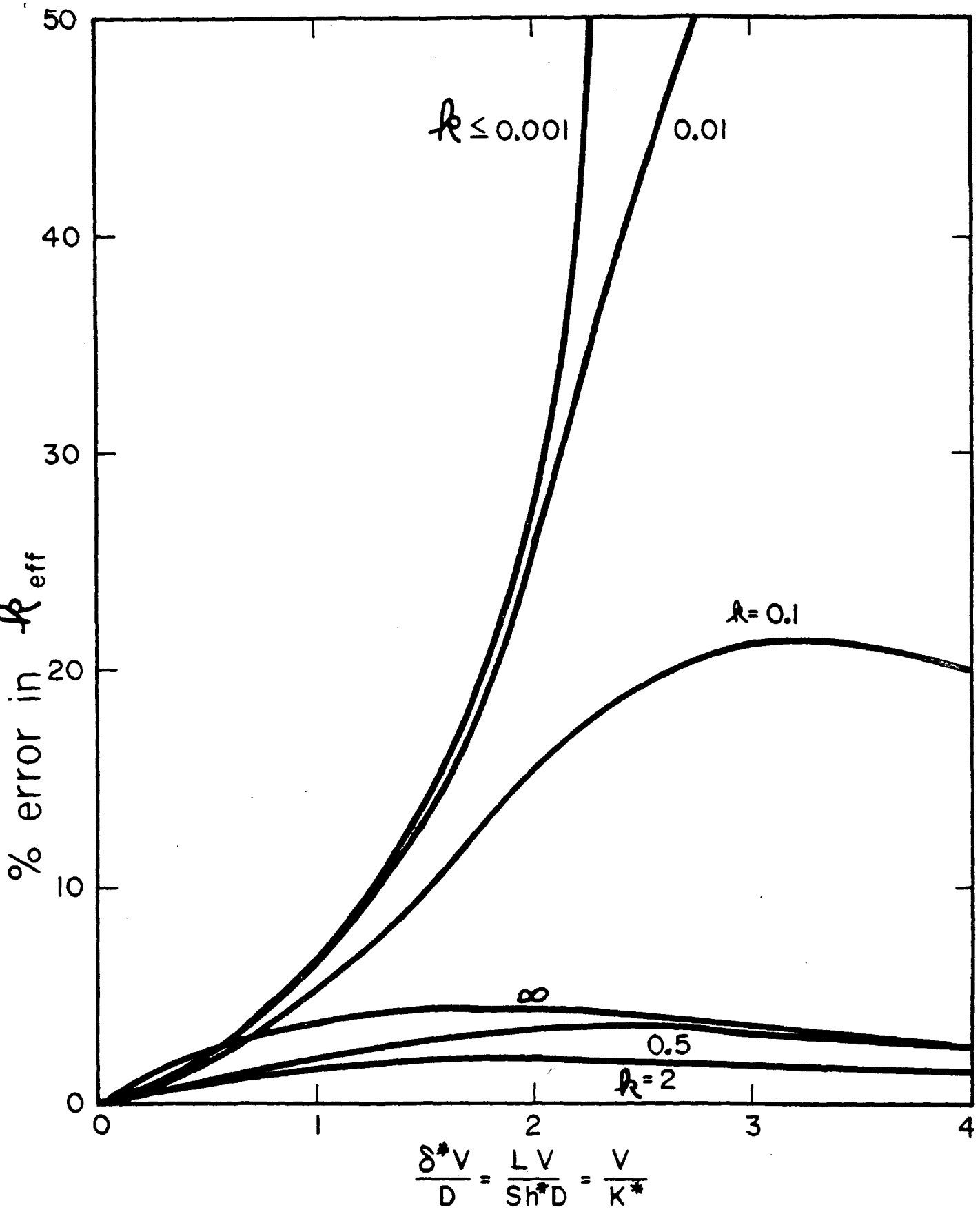

Figure 2. Error in calculating effective distribution coefficient by assuming $\delta' = \delta^*$ for liquid on rotating disk. From Eq. (16) and curve for Sc $\geq$ 10 in Figure 1.

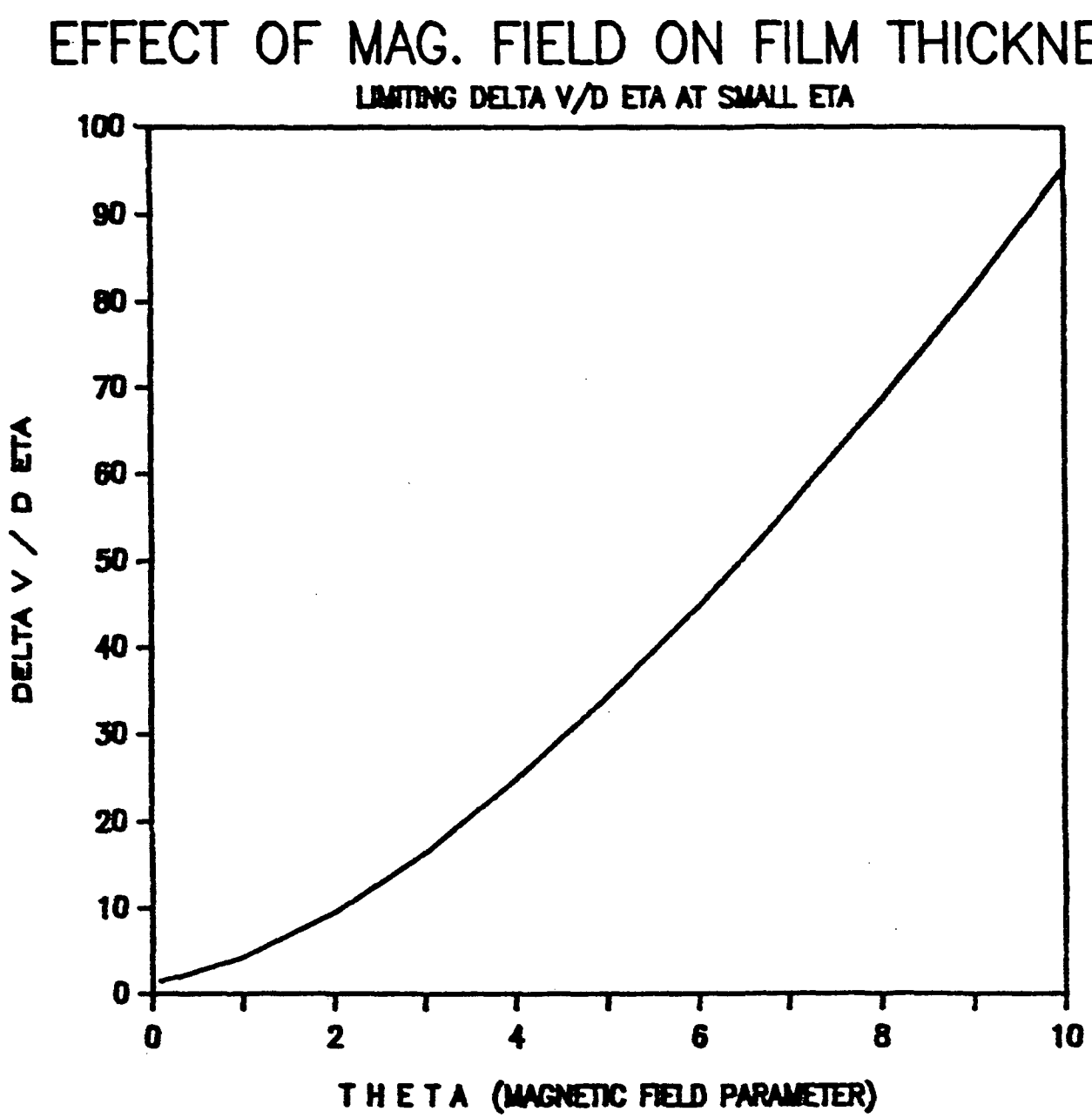

Figure 3. $\delta' v'_{cf}/D\eta$ vs. θ for a rotating disk with a magnetic field applied (calculated from [10]).

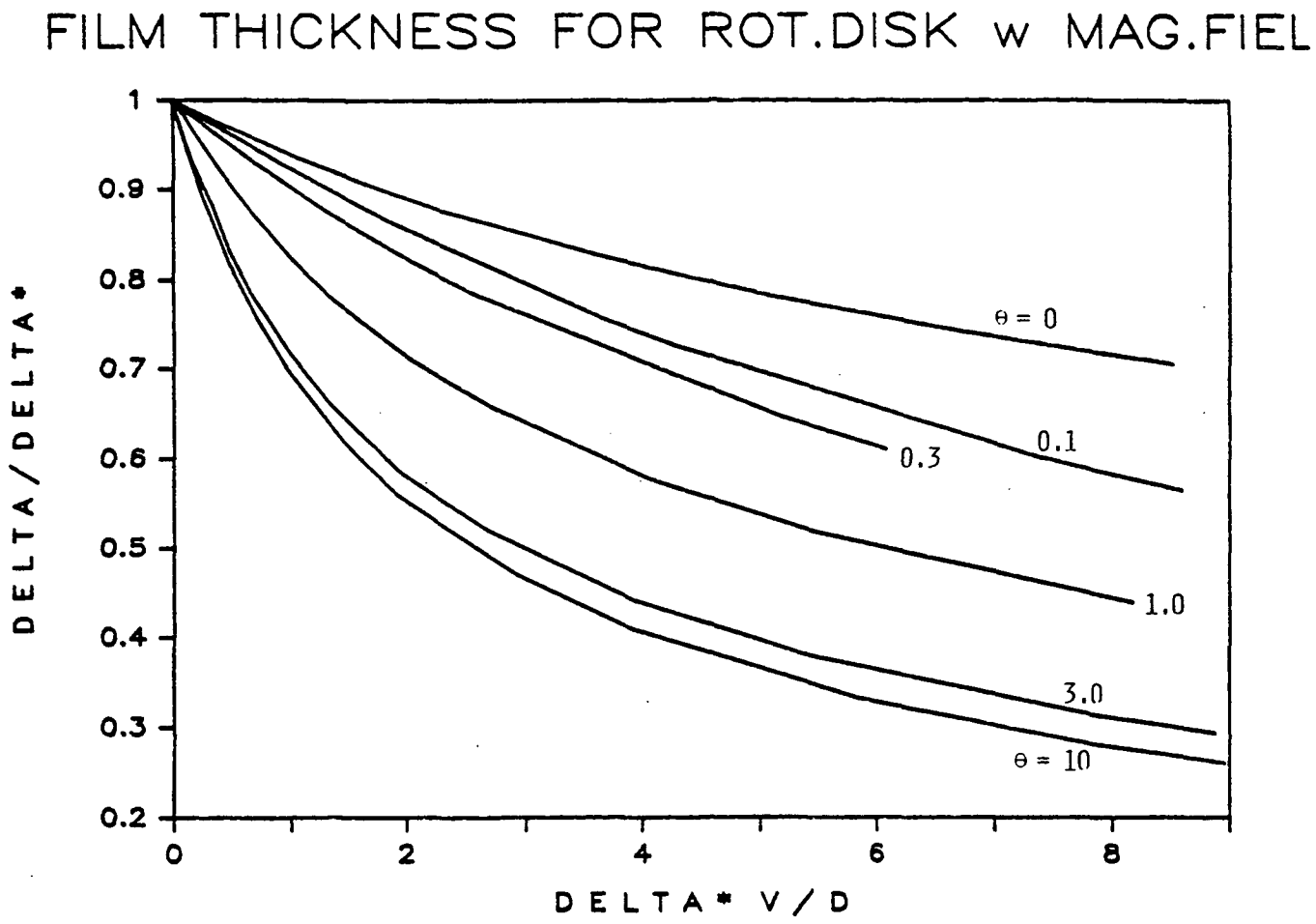

Figure 4. δ/δ^* vs. $\delta^* v_{cf}/D$ with a magnetic field applied of interaction strength θ (calculated from [10]).

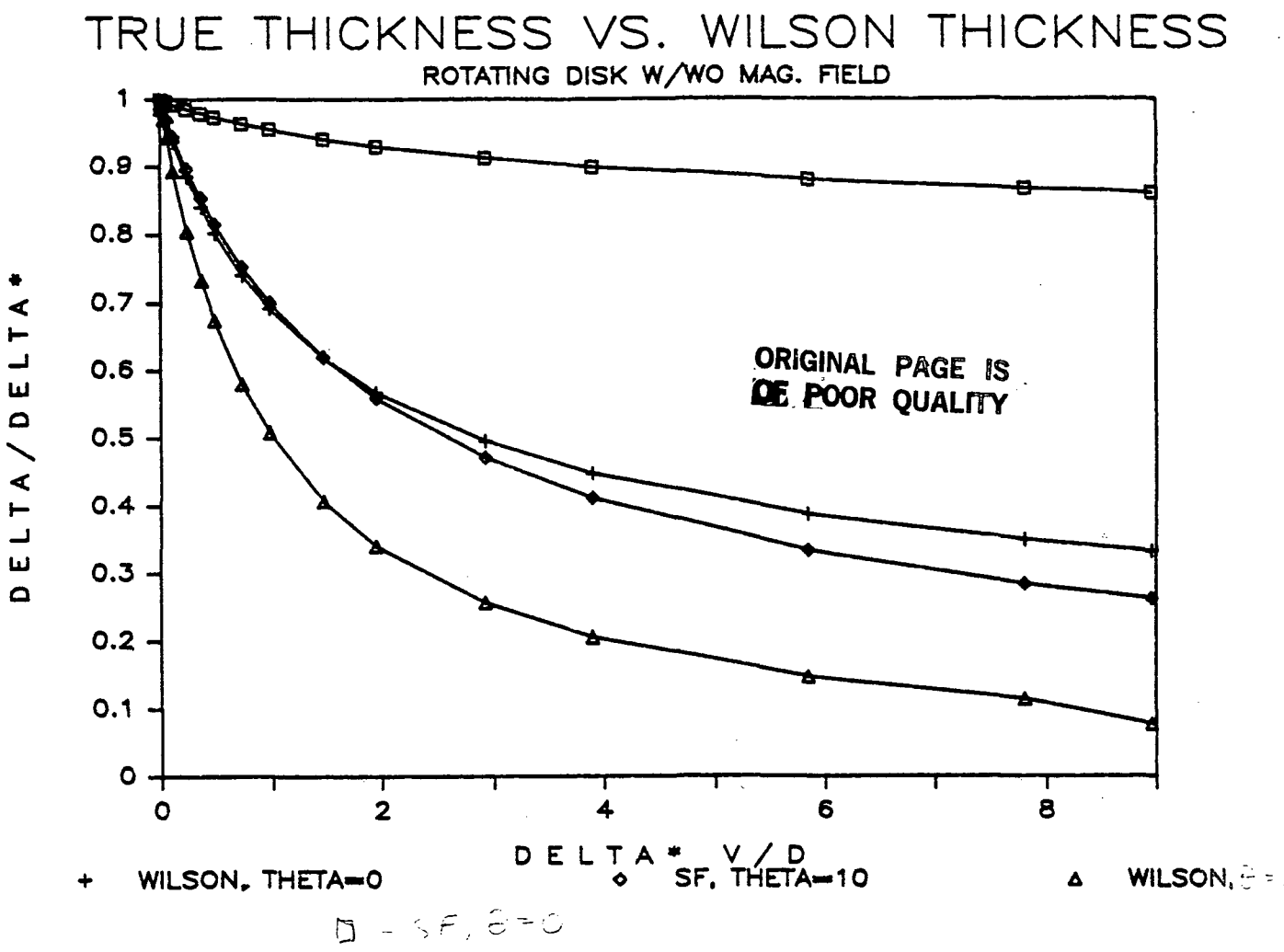

Figure 5. δ'/δ^* and $\delta_w'/\delta_w^*/v_{cf}'/D$ for a rotating disk (calculated from Eq. (15) without a magnetic field and from ref. [10] with a magnetic field).

□ - Stagnant film with no magnetic field.

◇ - Stagnant film with magnetic field, $\theta=10$.

\+ - Wilson film with no magnetic field.

△ - Wilson film with magnetic field, $\theta=10$.

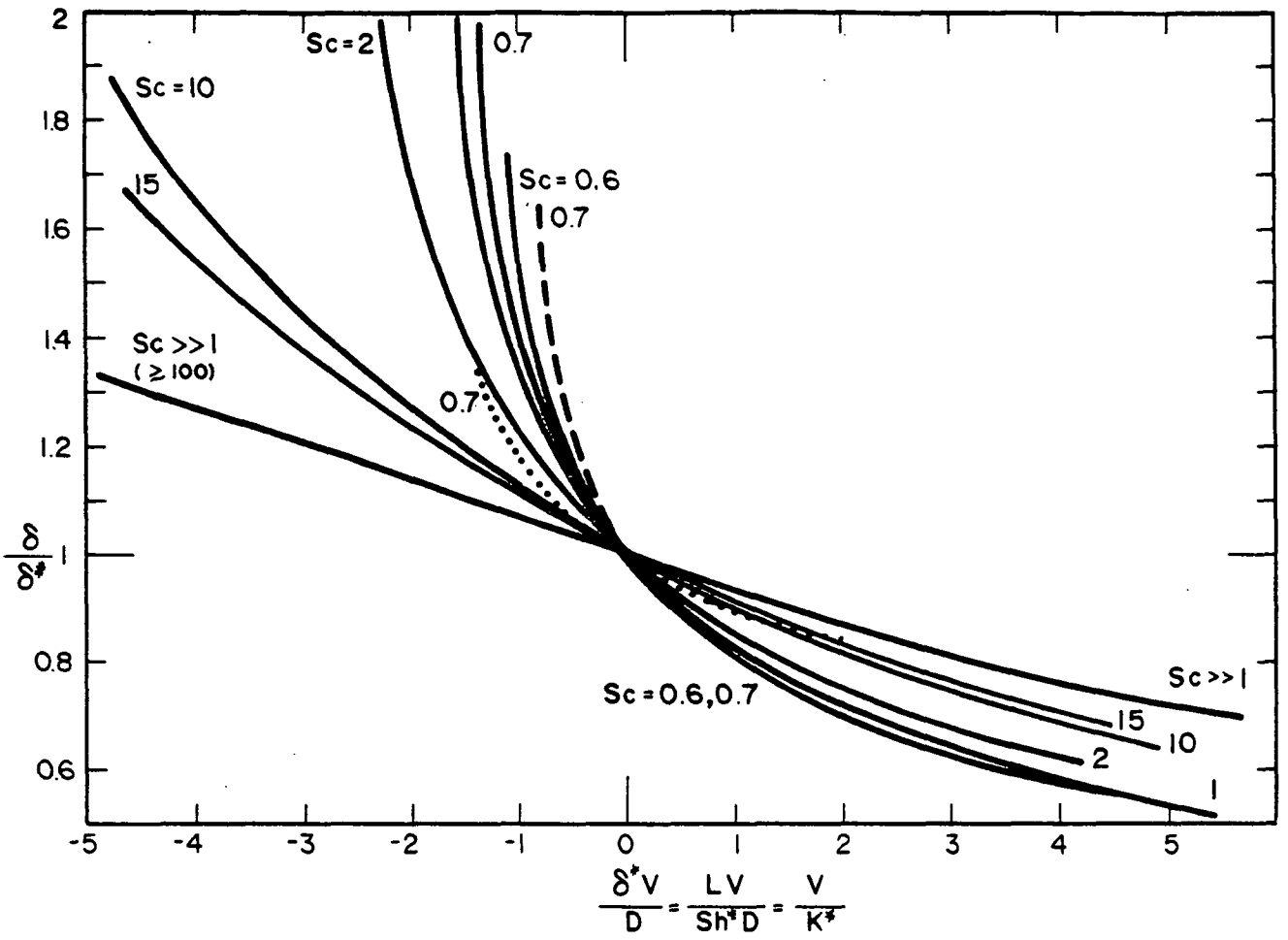

Figure 6. Theoretical results for laminar forced convection over a flat plate.

——— Constant concentration in crystal and in fluid at surface of flat plate, independent of distance x; $v'_{cf} \propto 1/\sqrt{x}$. Values for Sc >> 1 from references [11-16], for Sc = 15 from [17], 10 from [18], 2 from [12,19,20], 1 from [11,14,16-19, 21-25], 0.7 from [18,20,25-27], and Sc = 0.6 from [12,19,20].

– – – Concentration in crystal varying with $\sqrt{x}$, v'_{cf} with $1/\sqrt{x}$, and constant product of v'_{cf} and concentration in crystal. For Sc = 0.7 [27].

···· Constant v'_{cf} with Sc = 0.7 [26,27].

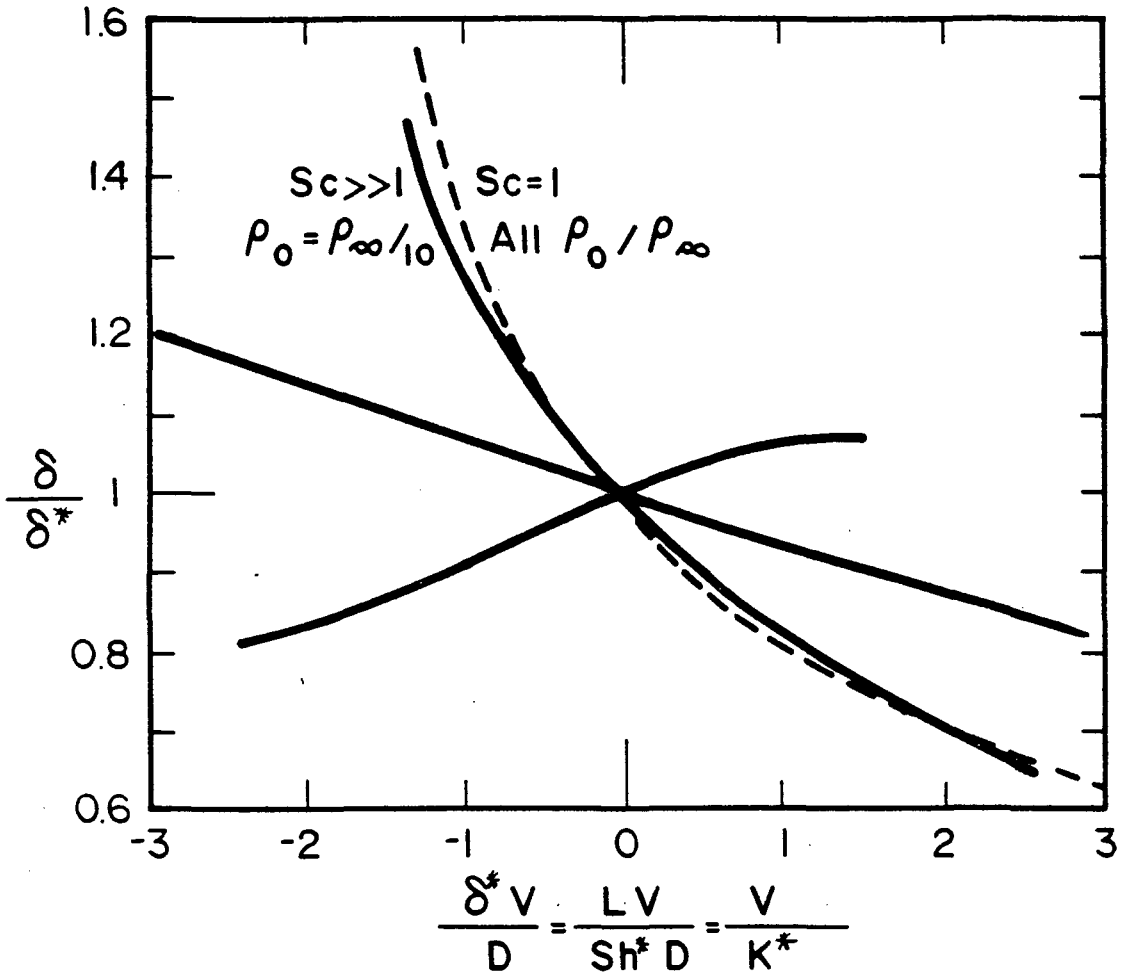

Figure 7. Laminar forced convection over a flat plate with variable density [16].

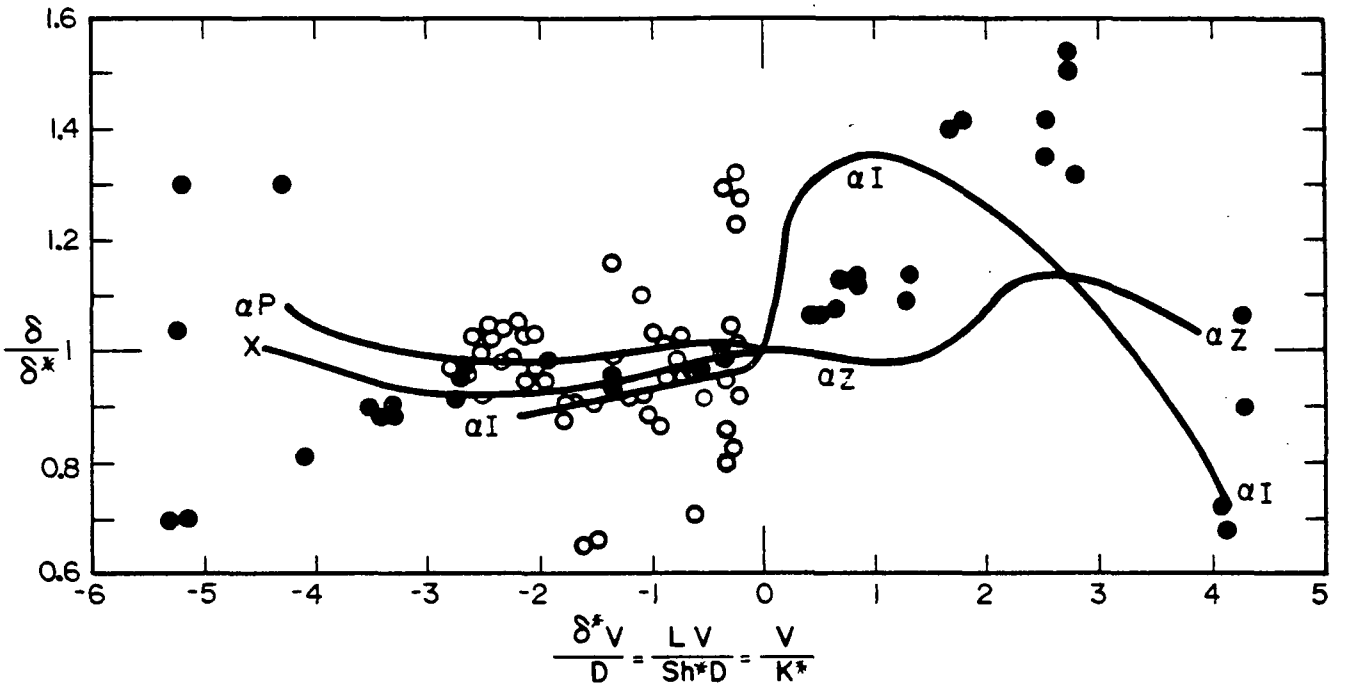

Figure 8. Turbulent flow of air over a flat plate with constant v'_{cf}.

——Theoretical treatments

X - Ref. [28]

αI - Ref. [29]

αP - Ref. [30]

αZ - Ref. [31]

○ - Experiments [32]

● - Experiments [19].

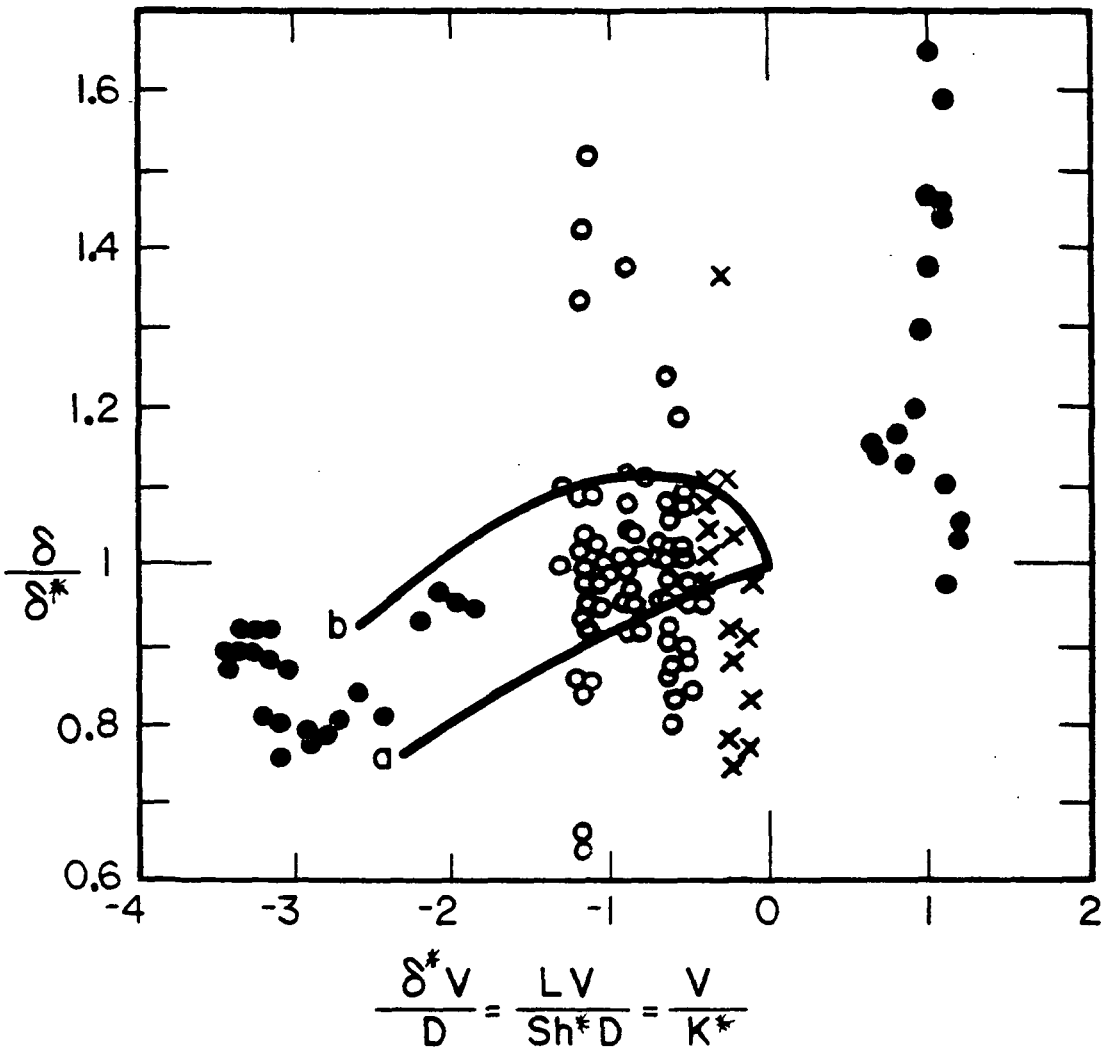

Figure 9. [illegible] flow of air over a flat plate with v'_{cf} decreasing [illegible] x.

——— Theoretical treatments for no growth for initial distance x_o, with free stream velocity independent of x [33].

a - $x/x_o = 1.15$, $Re = 10.4 \times 10^5$

b - $x/x_o = 1.77$, $Re = 7 \times 10^5$

● - Experimental for v'_{cf} α $1/x$, $U_\infty \alpha 1/x^{0.2}$, C_{A0} constant [34].

○ - Experimental for v_{cf} constant after laminar region with $v_{cf} \alpha 1/x^{0.2}$, C_{A0} approximately constant, U_∞ constant [19].

X - Experimental for v_{cf} constant after laminar region with $v_{cf} \alpha 1/x$ [19].

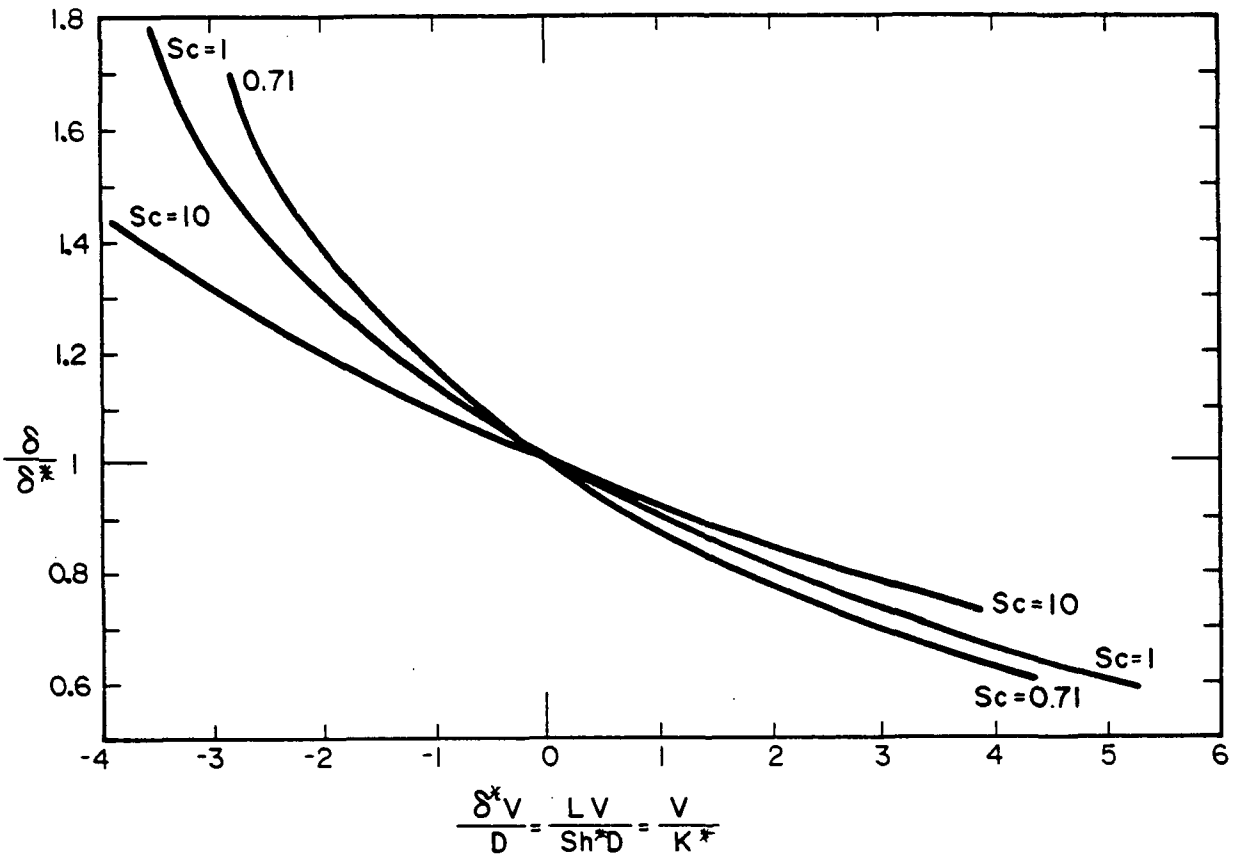

Figure 10. Laminar forced convection at stagnation point. Sc = 10 results from reference [18], Sc = 1 from [18,21,22,25], and Sc = 0.71 from [18,25,35].

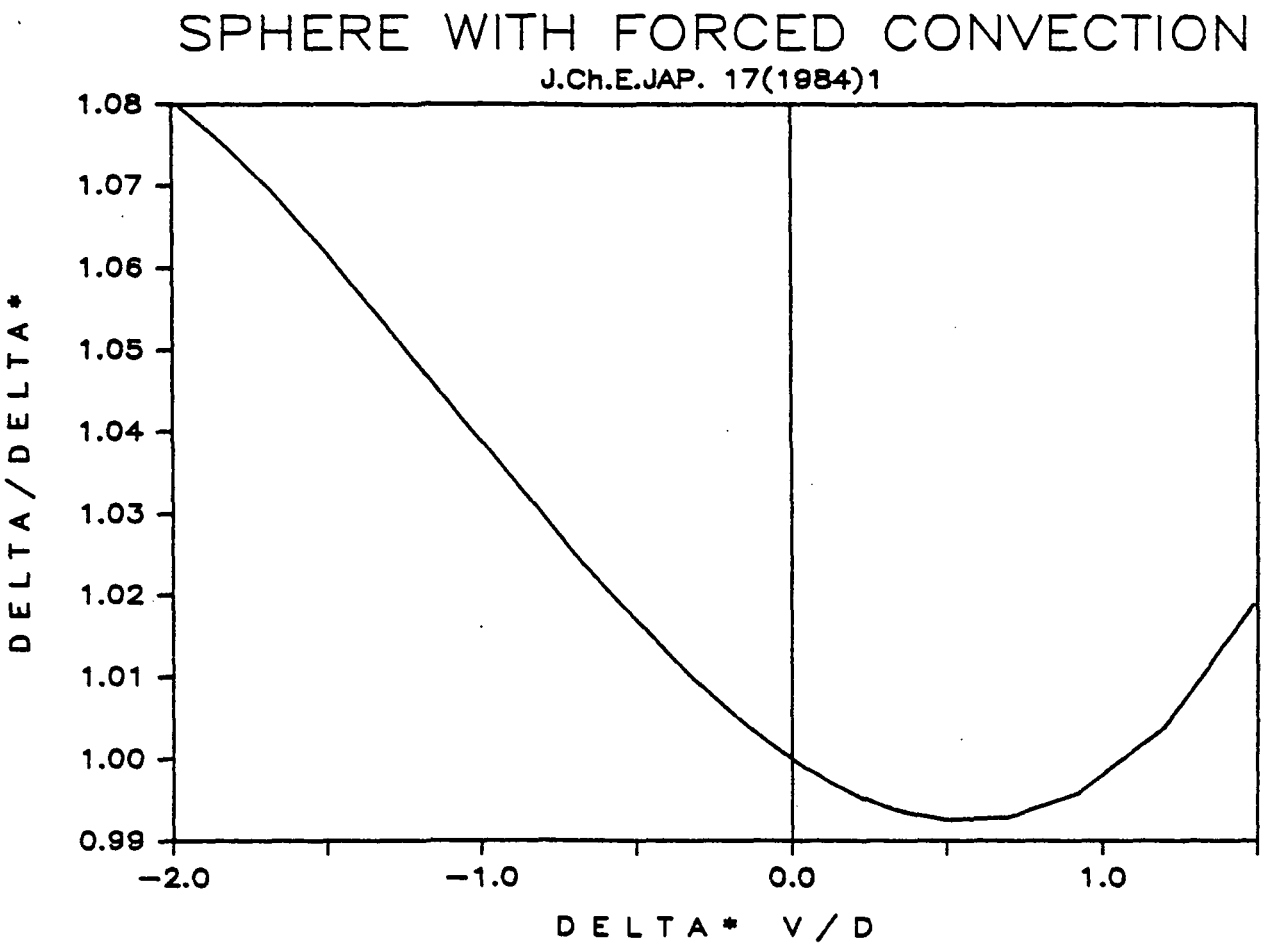

Figure 11. Laminar forced convection around sphere with uniform suction or blowing, for Re = 5 to 150 and Sc = 0.5 to 2 [36].

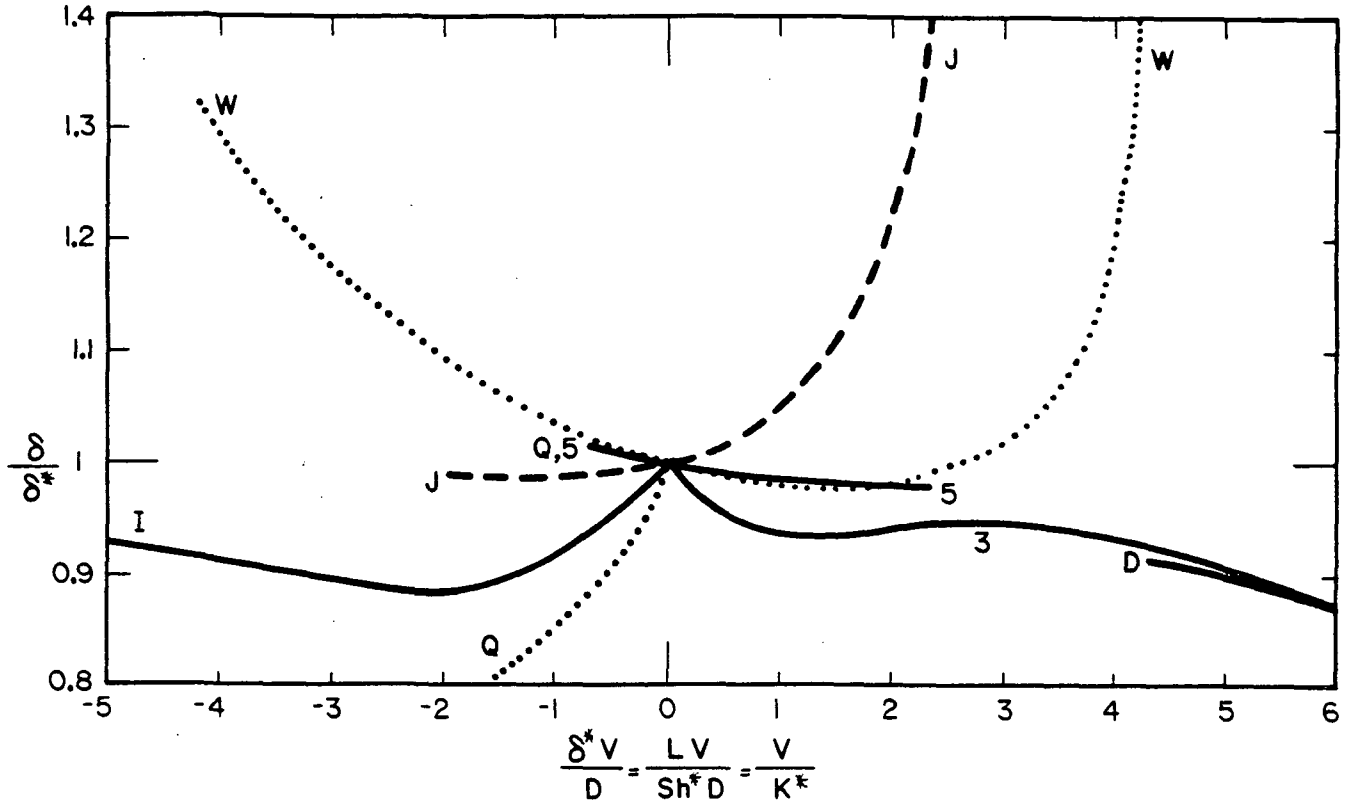

Figure 12. Theoretical results for free convection on a vertical flat plate.

——— Sc = 1, C_{A0} constant, $v_{cf} \propto 1/x^{0.25}$

I - Ref. [37]; D - Ref. [21]; 3 - Ref. [11];

Q - Ref. [38]; 5 - Ref. [39].

– – – Sc = 1, v'_{cf} constant; J - Ref. [40].

···· Sc = 0.71, C_{A0} constant, $V_{cf} \propto 1/x^{0.25}$;

W - Ref. [41]; Q - Ref. [38].

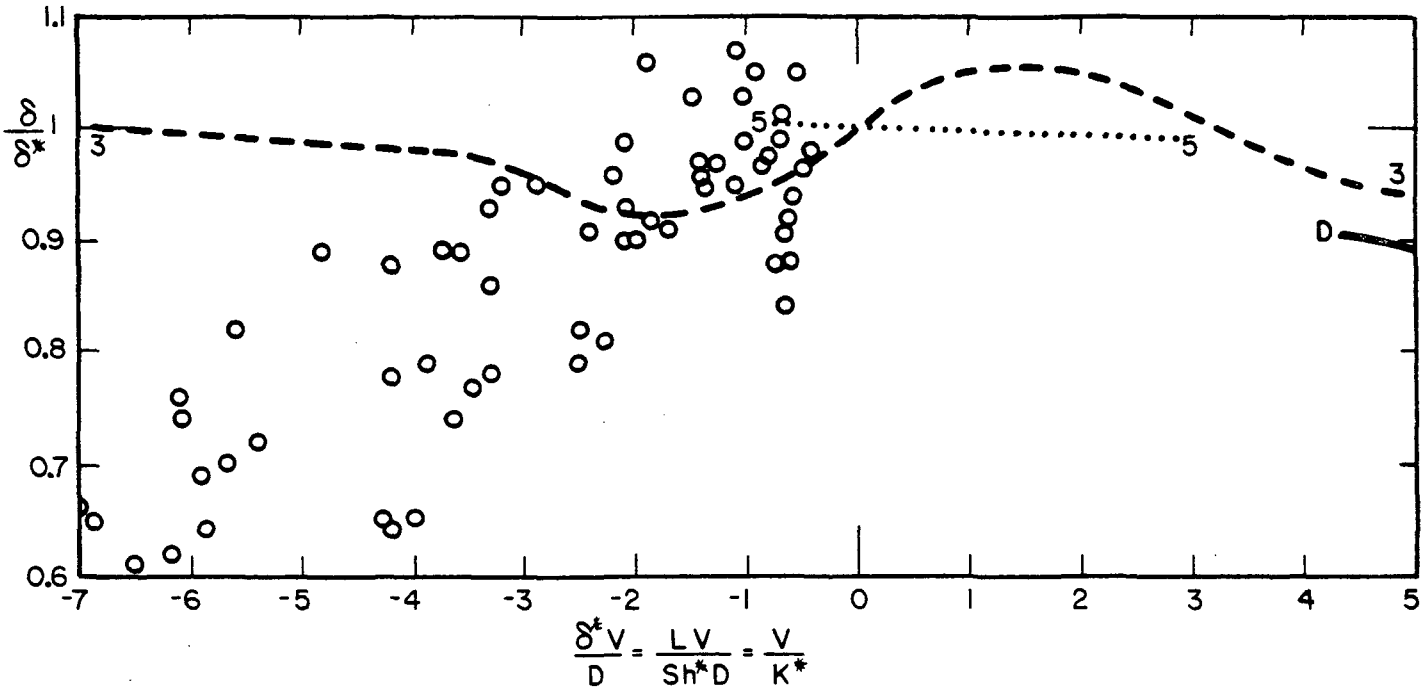

Figure 13. Free convection of liquids on a vertical flat plate.

— — — Theory for Sc >> 1 with C_{A0} constant, $v'_{cf} \propto 1/x^{0.25}$ [11].

——— Theory for Sc = 10 with C_{A0} constant, $v'_{cf} \propto 1/x^{0.25}$ [21]

• • • • Theory for Sc = 5 [39].

○ Experiments for Sc about 610 with v'_{cf} constant [42].

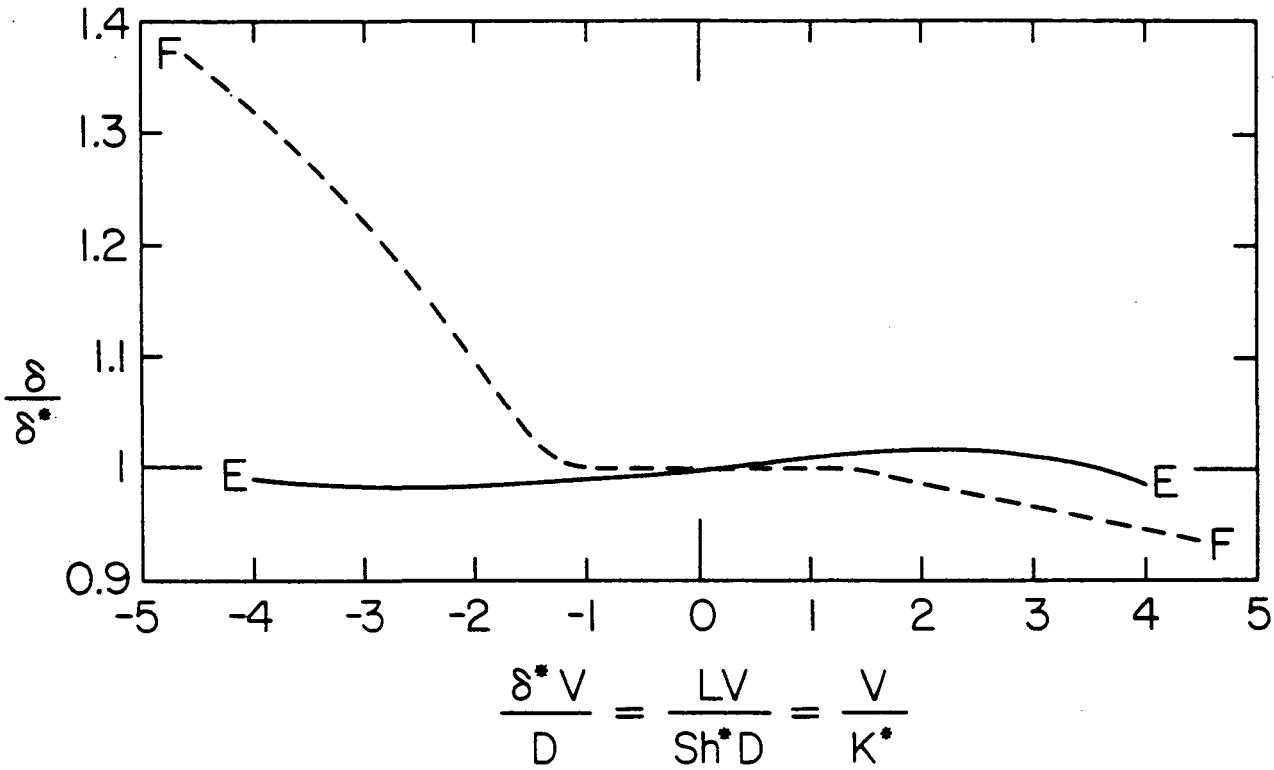

Figure 14. Theoretical results for free convection on the leading portion of a body.

F– – – Sc above about 2000 for three-dimensional flow without separation [43].

E—— Sc = 1, forward part of horizontal cylinder [44].

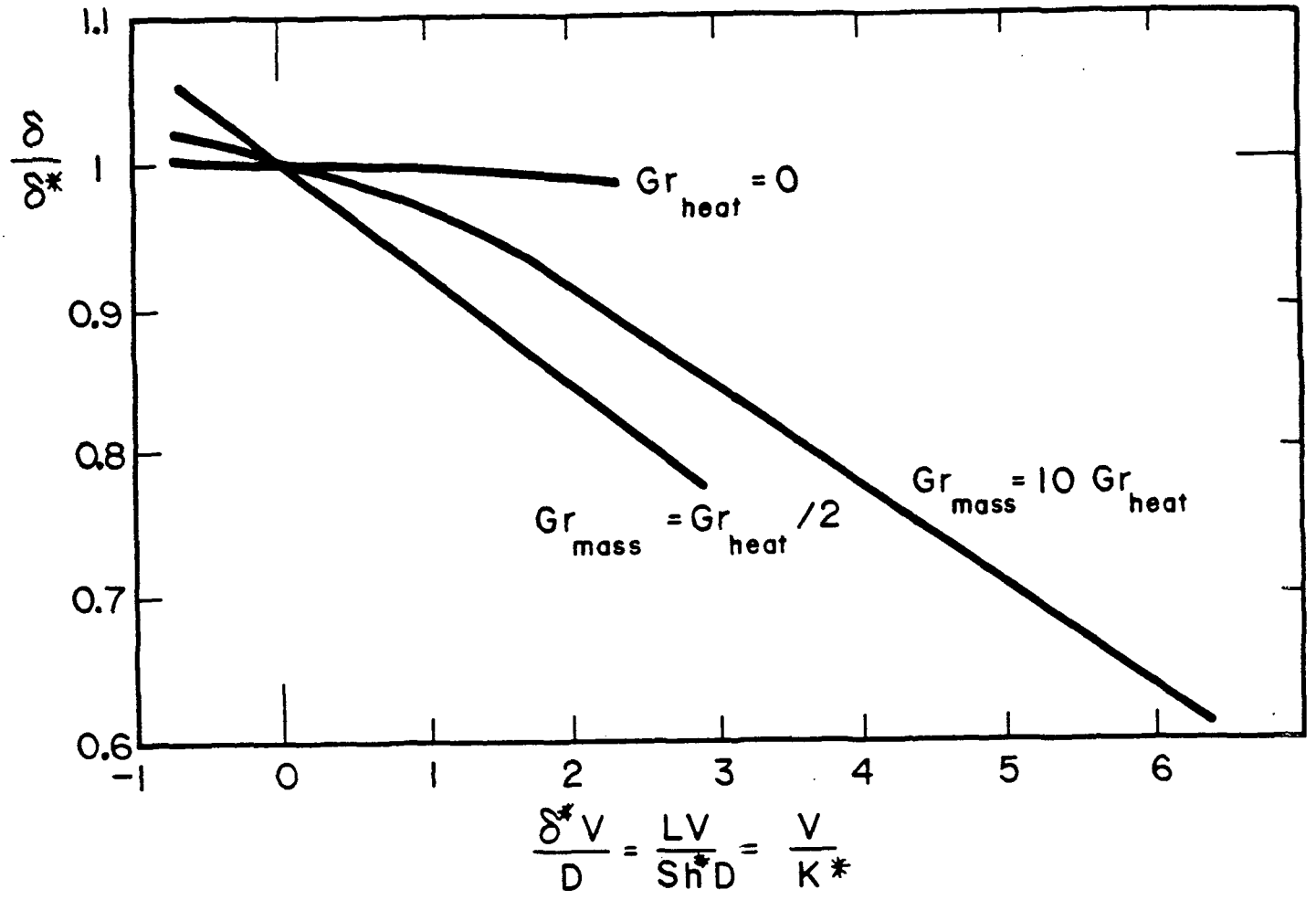

Figure 15. Theoretical results for free convection on a vertical flat plate with Pr = 0.2 and Sc = 5 [39,45]. Gr_{mass}/Gr_{heat} equals the ratio of density change caused by the concentration difference to that caused by the temperature variation in the fluid.

CLARKSON UNIVERSITY

Department of Chemical Engineering

THE EFFECT OF SPIN-UP/SPIN-DOWN ON TWINNING IN $In_xGa_{1-x}Sb$

A Doctoral

Research Proposal

by

L. Ruggiano

March , 1986

TABLE OF CONTENTS

CHAPTER 1

Introduction

I. III-V Compounds

Solid solutions of $A^{III}B^{V}$ semiconducting systems are important for many electronic devices. They offer advantages of composition-dependent band structures and properties different from simple binary compounds. By varying compostion, these properties can be altered to suit different purposes. Because of its band structure, $In_xGa_{1-x}Sb$ is promising for optoelectronic instruments such as photodetectors, light-emitting diodes and lasers (1,2,3). Optimum device characteristics occur at a composition of about 80% GaSb. However, in this composition range, $In_xGa_{1-x}Sb$ does not meet the electrical property requirements. The material is p-type with a high acceptor concentration whereas a low concentration (less than 10^{15} electrons/cm^3) n-type material with a high electron mobility is required (1,2,3).

For these applications, damage and inhomogeneity free crystals of high quality with low dislocation densities are required. Many different methods of growing these crystals in bulk have been published, but the end products were usually polycrystalline and/or compositionally inhomogeneous. Consequently, for the most part, bulk growth III-V alloys have been limited to scientific investigations. Extensive segregation occurs when bulk alloy melts are solidified, resulting in very inhomogeneous solids which are not suitable for any

devices.

A review of the pertinent literature exhibits the difficulties that previous experimenters have found in growing bulk crystals of $In_xGa_{1-x}Sb$ by many different crystallization techniques. These will be discussed in more detail later. Although films of this and other alloys have been produced by liquid phase epitaxy and chemical vapor deposition, bulk crystals are important because of their application as substrates for film growth and the need of bulk material for fabrication of many devices.

II. Objectives

The objective of the present investigation is to grow bulk single crystals of $In_xGa_{1-x}Sb$ and to learn about the processes causing polycrystallinity and the influence of operating variables on grain and twin generation and propagation. Twinning often occurs during crystal growth from vapor, melt and solution. In this research we are only concerned with growth from the melt. Many factors play a role in twin formation. The most extensively studied is mechanical stress. Twin formation and movement is a mechanism for plastic deformation in some materials. The other factors that may cause twin formation have not been thoroughly studied. Some of these that I propose to investigate are:

(a.) growth rate.

(b.) thermal stress.

(c.) feed composition.

(d.) foreign particles.

(e.) soluble impurities.

(f.) interface breakdown due to constitutional supercooling.

The crystals will be grown by the vertical Bridgman-Stockbarger technique with and without spin-up/spin-down applied to the ampoule.

III. Constitutional Supercooling

The primary difficulty in producing homogeneous single crystals of mixed III-V compounds from the melt can be seen upon examination of a typical temperature-composition phase diagram (Figure 1). If the lower melting component (InSb) is designated as the solute, its distribution coefficient is always less than unity and this component will be concentrated in the last segment to freeze. The melt adjacent to the interface becomes enriched in InSb. This extensive segregation generally leads to an inhomogeneous solid and can result in constitutional supercooling and interface breakdown.

Tiller et al. (5) first formulated the idea of constitutional supercooling to explain the breakdown of a planar interface to that of a cellular interface during alloy solidification. Only the concepts and results are presented here. For a more in-depth discussion of this topic the reader is referred to the original paper. A much more rigorous theory of stability criterion for the planar to cellular interface transition has been developed by Mullins and Sekerka (6), but physical insight can still be obtained from the classical concepts of constitutional supercooling.

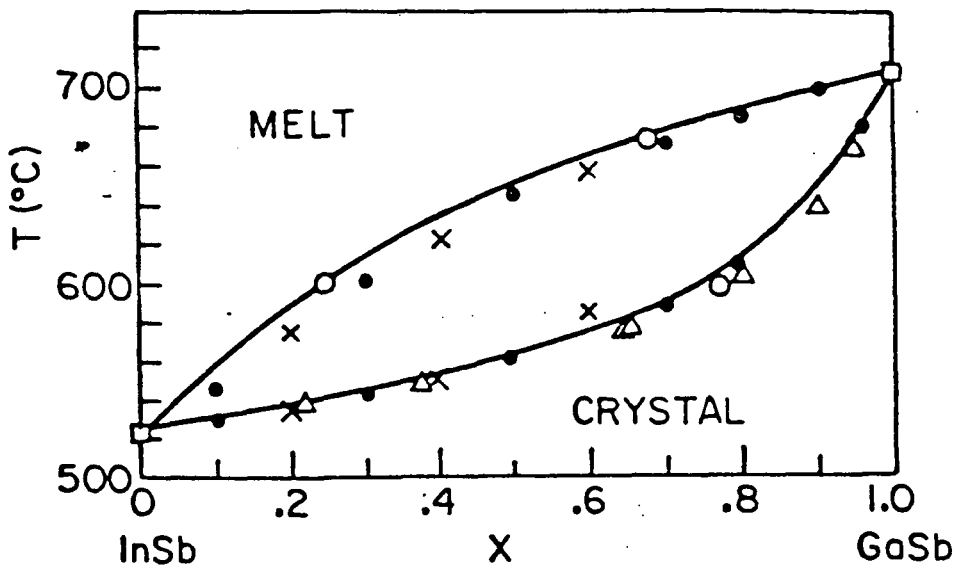

Figure 1: The InGa-GaSb psuedobinary phase diagram (37). X is mole fraction of GaSb.

Consider a melt of binary alloy of composition x_1. It is undergoing directional solidification at a constant freezing rate V under an imposed temperature gradient G = dt/dx. The solid is composed of more of the higher melting component (e.g. GaSb) than the liquid from which it solidifies. Consequently the higher melting component becomes depleted in the liquid adjacent to the solid/liquid interface. There will then exist a melting point gradient in the melt since the melting point T_m is composition dependent. When conditions of low temperature gradient and/or high freezing rate are imposed, the melting point can actually exceed the imposed temperature in melt adjacent to the interface. This can be seen in Figure 2. The region of constitutionally supercooled liquid is the shaded area between the imposed temperature T and the equilibrium melting temperature T_m. The condition for the occurrence of constitutional supercooling is given mathematically by:

$$G/V > (x_s - x_1)(m\ C_s / D\ C_1). \qquad (1)$$

where

x_s = composition of solid in mole fraction

x_1 = composition of liquid in mole fraction

m = slope of liquidus at the interfacial liquid composition x_1

C_s = Total molar concentration of the crystal

C_1 = total molar concentration of the melt

D = Binary diffusion coefficient

From equation (1) it is seen that avoidance of constitutional supercooling can be attained by maintaining a high interfacial melt

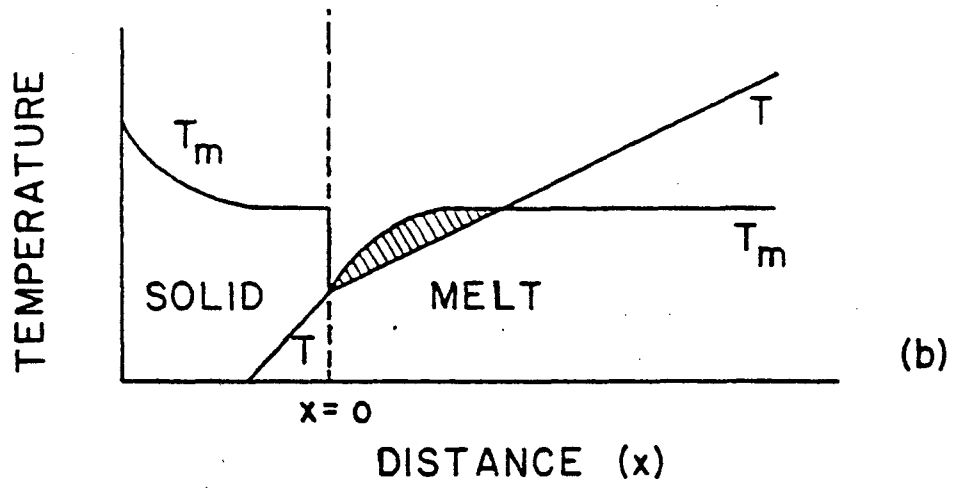

Figure 2: Constitutional Supercooling - The shaded region between the equilibrium melting temperature T_m, and the imposed temperature T, represents the region of constitutionally supercooled liquid.

temperature gradient G and low growth rate V.

Constitutional supercooling is responsible for the transition of planar solid/liquid interfaces to cellular and eventually dendritic interfaces. Under cellular interfacial conditions less solute is swept along with the moving interface than under planar interfacial conditions. Instead, much of the solute laterally segregates into cell boundaries. Dendritic interfacial conditions produce trapping, with most of the solute incorporated in the interdendritic regions. As can be deduced from the above discussion, interface breakdown has a very detrimental effect on crystal homogeneity and perfection. It leads to crystal defects such as inclusions, dislocations and possibly twins.

Free convection is a result of density variations arising from compositional and/or temperature variations in a gravitational or acceleration field. Uniform and time independent (steady state) flows can be useful since they decrease the buildup of compositional variations at the interface due to segregation, causing the growth to be less sensitive to small fluctuations in growth rate. However, time-dependent (transient, oscillatory and turbulent) flows are undesireable, because they generate variations in local temperature and flow velocity, resulting in growth rate variations and fluctuations in mass transfer causing the growing crystal to develop inhomogeneous compositional distributions and compositional striations parallel to the growth interface. Transients such as temperature fluctuations due to convection cause nucleation of twins and grains before interface breakdown has time to occur. If growth

conditions are such that the interface is near constitutional supercooling, then a momentary drop in temperature could cause a supercooled region in front of the interface and perhaps cause nucleation. Close to constitutional supercooling a sudden temperature drop can cause lattice mismatch by attachment of ordered groups of atoms in the melt adjacent to interface. A twin configuration is more likely for small perturbations, because it requires very little energy compared with grain boundary formation.

For the InSb-GaSb system Sen (7,8) plotted the critical G/V ratio versus the mole fraction of GaSb in the melt. For this purpose the binary diffusion coefficient D was assumed to be equal to 2 x 10^{-5} cm^2/sec. It can be observed from Figure 3 that a very large region of instability is encountered, resulting in a very small range of experimental conditions that will avoid constitutional supercooling. Sen (6) found that a temperature gradient greater than 40° C/cm produced thermal stresses in the $In_xGa_{1-x}Sb$ ingots that resulted in microcracks and other defects. On the other hand, smooth translation rates can be difficult to achieve experimentally when the rates are very low. This is due to the mechanical nature of such apparatus.

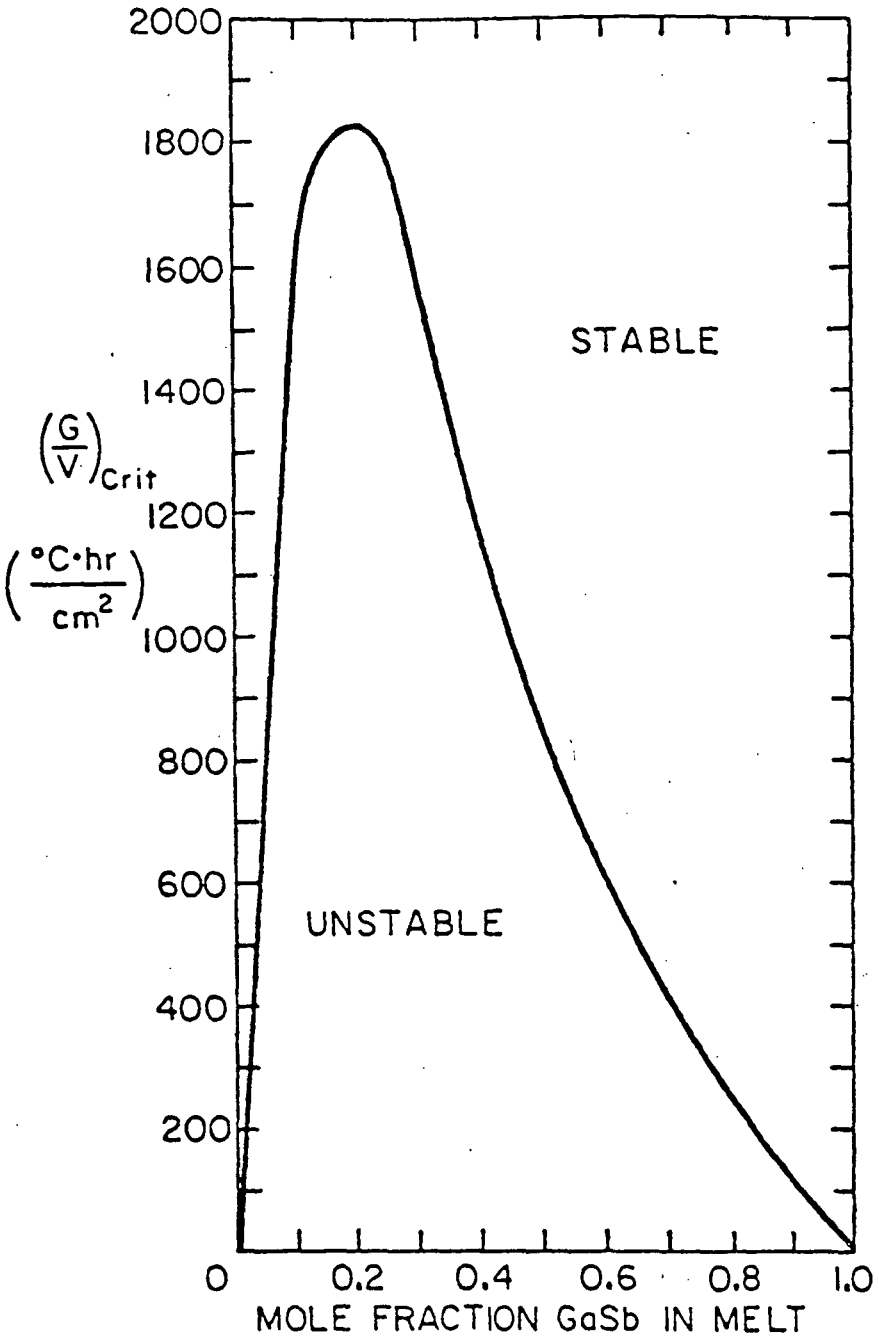

Figure 3: Critical G/V for constitutional supercooling in $In_xGa_{1-x}Sb$ calculated from equation (1) assuming

$D = 2 \times 10^{-5}$ cm^2 /sec (7).

CHAPTER 2

Literature Review

I. Twinning

Two joined single crystals are twins when the crytallographic orientation between them corresponds to low Miller indices and this orientation occurs frequently in growth or plastic deformation of the material. They require very little energy of formation and so are generally not considered grain boundaries, but a kind of crystal defect. Crystallographers believe that twin formation takes place when a crystal is unable to make an energetic distinction between the twinned and the untwinned extension. It is thought that twins occur randomly when the twin plane has a low energy (9). Twinning is not a random accidental phenomenon. Some materials frequently twin under particular conditions and not at all under other conditions. Twin planes are frequently utilized to obtain rapid crystal growth rates along a crystallographic direction parallel to the growth plane. They are one of the most common defects that occur during crystal growth, but their origin is not well understood. Twinning is a serious problem with the melt growth of group IV, III-V and II-VI alloy semiconductors. Compounds with the zinc-blende structure, such as $In_xGa_{1-x}Sb$, exhibit twinning with a geometry corresponding to 180° rotation about the (111) twin plane.

The definition of a twin can be quite ambiguous, because there are so many different types. Friedel (10) said a twin may be defined

as a polycrystalline edifice, built up of two or more homogeneous portions of the same crystal species in juxtaposition, and oriented with respect to each other according to well defined laws. Here homogeneous means that each portion can be referred to a single continuous lattice and that the constituent atoms are everywhere related in the same way to their nearest lattice points, i.e., each portion is a single crystal (11). Juxtaposition implies that the parts are in such intimate contact with each other over part of their boundary surfaces that they cohere, this cohesion being often, though not always, as strong as the internal cohesion of a single crystal (11). The requirement that the orientations be related according to well-defined laws is the most ambiguous part of the definition and has frequently given rise to dissension as to whether a particular specimen should be considered twinned. The components of a twin are frequently related to one another in one of the following ways (11).

1.) By reflection across a plane which is common to both parts.

2.) By rotation of one part by 180° about an axis common to both parts.

3.) By both of the above operations taking place simulataneously.

The plane normal to the axis of rotation or the plane across which reflection is imagined to have taken place is called the twinning plane and the axis as the twinning axis. The composition plane is the common plane of contact between two individuals of a twinned crystal. Optical examinations have revealed, however, that a true plane of contact does not exist in the case of interpenetrant

twins. The composition plane is often the same as the twinning plane, but not always. When not coincident, they are often at right angles to each other. Figures 4.1 to 4.6 show typical twinned crystals. Contact twins are joined at a face with atoms common to both parts (Figures 4.1 to 4.4). Interpenetration twins are shown in Figures 4.5 and 4.6. In this type the interface follows a number of different planes or may be quite irregular. The individual parts of interpenetration twinned crystals follow the same rules as for contact twins. They also have a common axis of rotation or common reflection plane existing as in the case of contact twins. Lamellar twinning is said to occur if individuals related in this way occur alternately. The twinned crystals of Figures 4.1 and 4.3 are as if one part of the crystal has been rotated 180° with respect to the other about an axis normal to the twinning plane. One part is the mirror image of the other about the twinning plane. In these two crystals the twinning plane and the twinning axis bear the same relation to the two parts of the twins. Figure 4.4 depicts a twinned crystal with composition plane parallel to (010), but the disposition of the parts can be only described by supposing the twinning axis to be either normal to (100) or parallel to their vertical axis. Therefore the twinning plane is (100) whereas the composition plane is (010), which is perpendicular to the twinning plane.

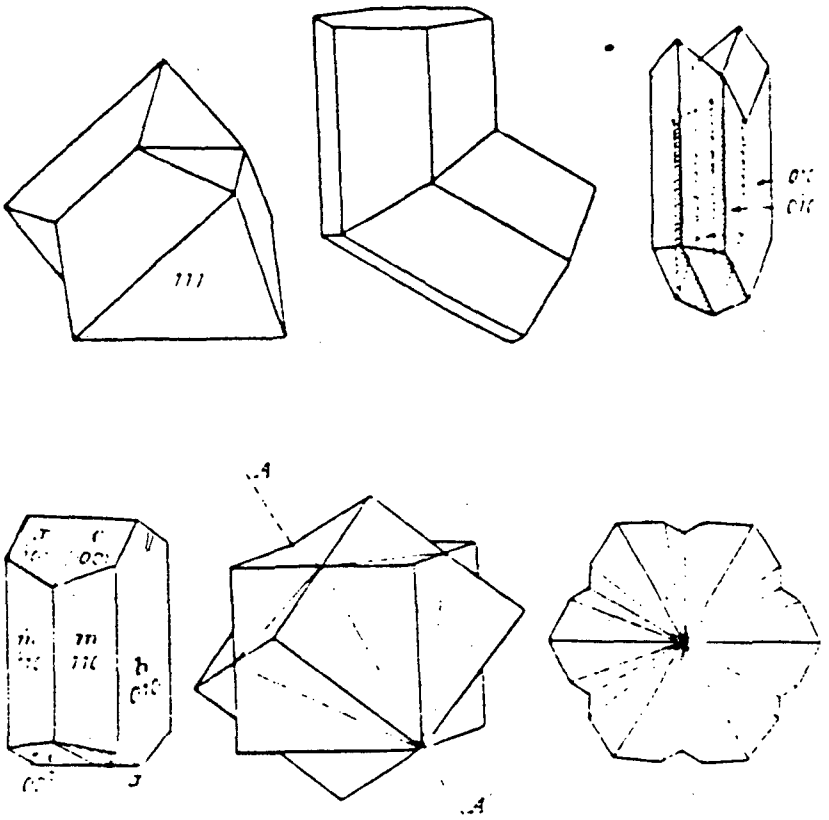

Figure 4: Examples of Twins (16)

4.1 Spinel twins with (111) twinning plane.
4.2 Hexagonal prism twinned on a pyramid face.
4.3 Arrowhead twin of gypsum.
4.4 Orthoclase twin (monoclinic).
4.5 Flourite interpenetration twin.
4.6 Interpenetration twin of potassium sulphate. Three individuals each one comprising opposite segments.

Sometimes more than two individuals are twinned together. In this case, when the twinning plane is parallel to a pinacoid, every alternate member of the series is similarly oriented. Whereas when the twinning plane is inclined, as is the case of a prism or pyramid face, a cyclic grouping results. Twinning involving more than two individuals is known as multiple or mimemic twinning. If this kind of twinning is repeated several times, so that each part is of microscopic thickness, then the outer surface of such a crystal appears to be striated. This is known as polysynthetic twinning.

Twin formation takes place either when the material is mechanically stressed (by applying a load on it) or during its growth from solution, melt or vapor. Mechanical twins are formed when the stress causes the crystal to dislocate through a distance which is not a multiple of the unit cell dimension (i.e., via a partial dislocation). In this work we are only interested in growth twins. There are two views on the origin of growth twins (11):

(1.) Growth accidents at the interface, because of high growth rates (13), impurities (14, 15) and interfacial perturbations leading to dislocations acting as sites for twin formation. The implication here is that twinning might occur directly as the crystal grows from the melt, i.e., during deposition of individual atomic layers. Twinning in the diamond or zinc-blend crystal structure is always observed with one of the {111} family of lattice planes acting as a twin plane (111). In the diamond lattice there are four types of such octahedral planes belonging to the same family inclined at

$70^{\circ}32'$ to each other. Twinning about a (111) plane is a simple stacking fault. It gives a perfect fit of the lattices on either side. Therefore it leaves all distances between nearest neighbors and all bond angles undisturbed. Consequently, very little energy is required, only that due to interaction between second nearest neighbors, to initiate such twinning. Therefore a single crystal growing with a certain crystallographic orientation can readily swing over to one of four other orientations by this mechanism. Temperature fluctuations in the melt may be sufficient to initiate such twinning.

Quite often the consequence of twinning on the growth mechanism and kinetics can be explained by the reentrant corner effect. The concept is based on the premise that a pair of twins form a reentrant corner at the growth interface which acts as a favorable nucleation site for new steps. The reason for the formation of favorable nucleation sites at the reentrant corner has been explained by Sen (16) in the following way. The twins considered are depicted in Figure 5. These twins come into contact at corner A. If a growth layer is started on face B or C due possibly to a screw dislocation or to two dimensional nucleation, then the growth layer spreads on surface B. This growth layer will then reach corner A where it acts as a nucleation site for atoms on surface C. Growth proceeds on surface C once a layer of atoms nucleates at corner A. Because the twins are at an angle to each other, the growth layers on surface B and C do not match, leaving a ledge at position A. This ledge (step) now provides nucleation sites for growth on surface B. Similarly the

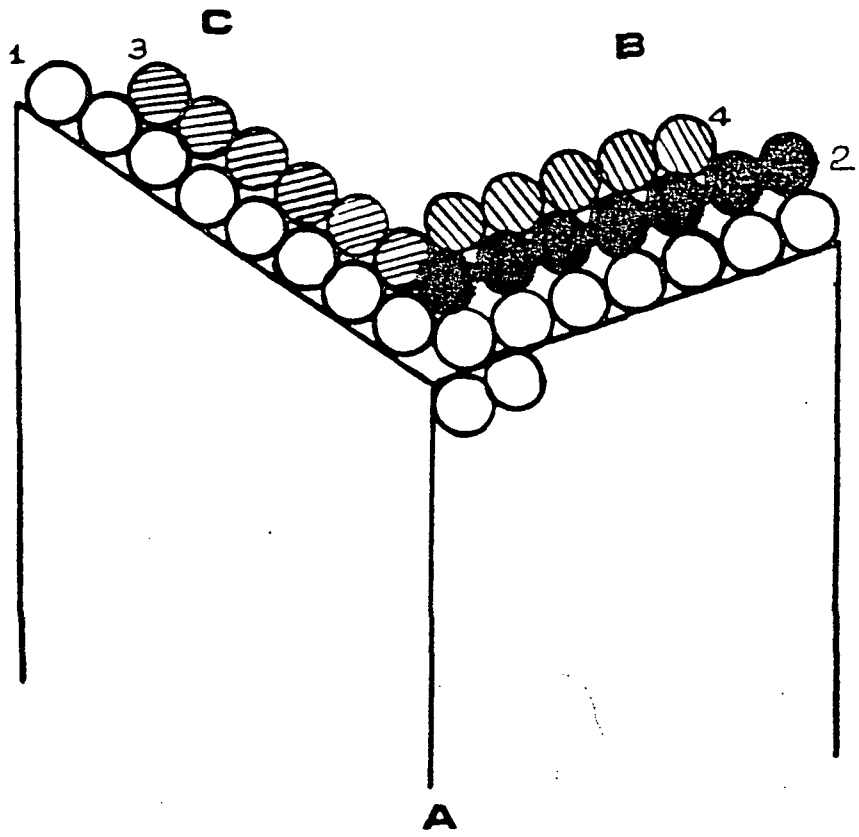

Figure 5: Reentrant corner effect. The twins form an open figure with faces B and C. Face C provides a source of steps for B and vice versa. The numbers denote the sequence of layer formation (16).

growth layer on surface B forms a ledge at A which provides favorable nucleation sites for growth on surface C. Growth then proceeds in this fashion with the help of ledges and corner A. Wagner and Brown (17) postulated the conditions for crystal growth using the twin plane reentrant corner effect:

(a.) Growth form of the material should be faceted.

(b.) Twin boundaries should be present, caused by a fault in the layer sequence during growth by plastic deformation or by an accidental meeting of crystals at the twin angle.

(c.) Twins should form a reentrant step where the twin boundary terminates at the faceted growth interface.

It is also thought that twins might be caused by local disturbances such as the presence of foreign particles. Such particles may appear anywhere on the growing front and a twin can thus start within an ingot (15). On earth the particles with a density higher than the melt will tend to settle down near the solid/liquid interface due to gravity. If convection is present particles will move along the convective flow path and bounce repeatedly on the solid/liquid interface. Twins might be generated when they come in contact with the interface. When the convection is suppressed, as by the imposition of a magnetic field, the particle motion is suppressed inside the melt. Due to gravity they will tend to settle down at the interface. Therefore it would be expected that under gravity conditions the twins would all emerge at the beginning of growth and then their number would gradually decrease as solidification progresses. In the Skylab (19,20,21) grown samples of

$In_xGa_{1-x}Sb$ there was a 70% reduction of straight twin boundaries as compared to earth grown samples. Due to the lack of gravity any particles present inside the melt in the Skylab would have remained dispersed in the melt and would have contacted the surface only when the interface reached them, preventing the particles from settling on the interface unless surface driven convection was significant.

(2.) The second view proposes that growth twins are sometimes or even always of mechanical origin (18). Thermal stresses in solidified crystals that are near the melting point can cause crystal defects. Ge and Si (15), which are known to plastically deform, are thought to fault during constrained growth (growth in a crucible). The twins Sen (7) saw in grown ingots of $In_xGa_{1-x}Sb$ were believed to have been generated after solidification when the solid was still hot and capable of plastic deformation due to the thermal stresses internally and within the crucible. More twins were formed when a magnetic field was not applied or partially applied compared to ingots where the field was applied for the entire growth period. Since the magnetic field did not completely suppress formation of twins, both factors (free convection and thermal stress) were probably responsible for the generation of twins.

II. Literature Review On $In_xGa_{1-x}Sb$

Sen (7,8,21,23) produced bulk ingots of $In_xGa_{1-x}Sb$ by the vertical Bridgman-Stockbarger technique. Ampoule travel rates were 4.0 and 8.0 mm/day. Electron microprobe analysis performed on the grown ingots showed no significant radial composition gradients. The

average number of grain boundaries increased approximately 30% when the mole fraction of InSb in the feed was increased from 0.1 to 0.5. Sen explains this as an increase in the segregation of solute which causes the development of a solute rich layer adjacent to the solid/liquid interface. As can be seen from the temperature - composition phase diagram of Figure 1, a decrease in the melting point is associated with an increase in the concentration of InSb. This causes an acceleration in growth and more rapid nucleation. The average number of twin boundaries was found to be less composition dependent. Lower G/V ratios produced more twins and grain boundaries than higher. Increasing the temperature gradient to 40 - 50° C/cm did not yield single crystals. This increase resulted in a fine grain structure due to increased thermal stress with cracking and dislocations, perhaps leading to new grains and twins. Increasing the temperature gradient probably also generated irregular turbulent convection in the melt giving rise to larger growth rate fluctuations.

The total number of twins and grains were much less in the case of an applied magnetic field of 2 KG than otherwise, and when twins were generated it was to a much lesser extent in the presence of a field. The magnetic field reduced formation of twins probably by inhibiting convection and therefore reducing temperature fluctuations in the melt. The magnetic field did not completely inhibit the formation of grain and twin boundaries indicating that their formation was also caused by compositional or thermal stresses.

Sen also found that when twins nucleated, sometimes new grains were seen shortly thereafter, but in smaller quantities. Twins grew out quickly, because they are geometry dominated rather than interface (shape or position) dominated. Grains grew out slowly suggesting an only slightly favorable curvature of the interface.

Annealing (23) of the grown ingots at a temperature of 500°C (80% of the melting point) with a load of 66 grams (0.45×10^5 dynes/cm^2) on top of the ingots for a period of ten days resulted in a 40 to 80% decrease in the number of curved boundaries and a 30 to 60% increase in the number of straight twin boundaries for all feed compositions of alloy. No apparent changes in grain structure were observed when annealed with no load and the only single crystal grown during this research showed no change even with load. The reduction of the number of grain boundaries can be the result of grain boundary movement at high temperatures and under plastic deformation or grain growth. There could be some annealing twins also generated, associated with grain growth under stress. Results of annealing experiments suggest that the generation of twins during growth occurred immediately after solidification when the solid was still hot and plastic. Since it is known that the shear stress required for twinning at high temperature is very low, the mechanical stress arising from solidification in a crucible might be sufficient to generate the observed twins (23).

Sen (7) also grew $In_xGa_{1-x}Sb$ by the Gradient Freeze Method (7). Grain selection was poor and many more twins were generated in this method than by the vertical Bridgman-Stockbarger technique.

Therefore no quantitative studies were made. The composition of the grown ingots was fairly homogeneous both radially and axially up to a point where compositional fluctuations started to develop. This is because as the interface advanced upwards the effect of the cooler was less and less felt, thereby reducing the temperature gradient at the solid/liquid interface, favoring constitutional supercooling.

In order to provide information regarding the theory that free convection induced compositional fluctuations cause grain generation directional solidification of $In_xGa_{1-x}Sb$ alloys in a "gravity-free" environment was undertaken. Three different compositions (x = 0.5, 0.7 and 0.9) of the alloy were directionally solidified by the Gradient Freeze technique in Skylab missions SL3 and SL4 and for comparison on earth in horizontal and vertical orientations (19-22). The average acceleration was about 10^{-4} of the earth's gravity g_e, with occasional fluctuations as high as 10^{-3}, which should have been sufficiently low that free convection was negligible. The objective was to see if space processing (where natural convection due to gravity is practically zero) offers any advantages for single crystal growth of concentrated alloys by melt techniques.

Microstructures of space-processed ingots were superior to those of vertically and horizontally earth-processed ingots with the vertically processed being slightly better than the horizontally processed. Straight twin boundaries were 70% less in the six Skylab ingots than in the six earth processed ones. The number of grain boundaries and irregular twin boundaries (exclusive of straight twin

boundaries) were approximately 18% less in the Skylab ingots. On earth, new grains and twins nucleated during growth while in space almost all grains and twins propagated from the unmelted portion of the extremely dendritic feed rod. The x-ray and electron diffraction studies revealed that the twin planes were {111} and preferred orientations were <211>, <110>, and <321> (in decreasing order of frequency). This and twinning in dendrites in the initial cast material led Sarma to believe that the growth mechanism in this case may be similar to that of dendritic growth in Ge, Si and InSb (15). This is a self perpetuating reentrant angle associated with multiple twinning. In the slowly refrozen regions of the space processed ingots, the twin boundaries appeared to jog sideways in an attempt to realign themselves perpendicular to the solid/liquid interface. The curvature of these twin boundaries suggests energy minimization by alignment perpendicular to the solid/liquid interface during solidification in a manner commonly observed for grain boundaries. On earth, the number of twins initially increased and then decreased with time. On earth and in space, twinning decreased as the feed composition of InSb increased (19,20,21,22).

Joullie (2) prepared bulk ingots of $In_xGa_{1-x}Sb$ alloys by the vertical Bridgman-Stockbarger technique. Ampoule travel rates were 1, 0.45 and 0.25 mm/hr. At 1mm/hr a second phase arises, generally in the form of inclusions in the nearly homogeneous matrix. At the two lower rates, the ingots grown are of one phase which provide radially homogeneous samples. Woolley et al. (24) produced solid solutions of various compositions of InSb-GaSb. The resulting crystals were inhomogeneous and polycrystalline. The authors attributed this to

the effects of constitutional supercooling. Coderre and Woolley (25) produced ingots of InSb-GaSb by the vertical Bridgman-Stockbarger technique. Due to constitutional supercooling the ingots were polycrystalline, but homogeneous in cross-section at all points.

III. General Literature Review

Skylab 3 and 4 missions also included the growth of undoped, tellurium and tin-doped InSb in the "Multipurpose Furnace" on earth and in space (12,26). The Te-doped space-grown crystals will be now described. The surface of the regrown crystals in the vicinity of the seed exhibited several bands of differing width oriented normal to growth direction. These were identified as external boundaries of (211) rotational twins which are frequently encountered in InSb grown in the <111> direction. Each band is the result of two consecutive rotations by 60° of the (111) plane normal to the growth direction. Etched segments of (211) surface orientation show that some twins propagated across the entire crystal and some terminated in the crystal and others deteriorated to grain boundaries. Because of a concave interface, nucleation during growth was essentially restricted to the outermost peripheral part of the growth interface. Rotational twin formation initiated by a nucleus having a 60° misorientation was explained as a result of misoriented nucleation at the crystal periphery. Crystals grown in space exhibited a dislocation density 40% smaller than those in the earth-grown segment. It was concluded that steady-state segregation and homogeneous dopant distribution was achieved under zero gravity conditions. In ground-based identical experiments the dopant profile

indicated a steadily increasing dopant concentration which reflects the presence of slow convection caused by unavoidable lateral thermal gradients (12,26).

Walter (27) describes the defect properties of InSb single crystals prepared by a containerless technique on Skylab. Defect properties of space-grown crystals were compared with Czochralski-grown crystals that were used as seeds. Undoped and selenium-doped crystals of InSb were grown in this study. In Skylab, Czochralski grown crystals were partially backmelted in a gradient furnace so that large drops of uncontained melt were formed at the end of the seed crystals. These drops were directionally solidified during controlled cool-down of the furnace after a one hour soak period.

Walter's (27) earth-grown InSb exhibited 10^2-10^3/[illegible] foreign particle inclusions. The larger [illegible] were frequently [illegible] and served as nucleation sites for grains and twins. The dislocations in the Czochralski-grown crystals were randomly oriented and curvilinear. The InSb crystals grown in space were very different. Walter (27) describes them as remarkably homogeneous. The density of inclusions was greatly reduced, presumably because foreign particles accumulated during soak at the remelt boundary and at the melt surface. Dislocations originating from particles at the seed boundary were thought to be the cause of a sudden increase of dislocation density in the first part of regrown material. Rectilinear dislocations (pure edge and 60° type) were observed exclusively in the bulk of the space-grown crystals. Since

larger inclusions were absent, few defects were generated and the density of dislocations decreased along the axis of the samples due to the outgrowing of rectilinear dislocations that were inclined to the growth axis. Increasing radial thermal gradients were thought to have caused the increase of dislocation density in the crystal section solidified last. (Generation and multiplication of dislocations due to radial thermal gradients becomes appreciable at gradients of about 10-15°C/cm (27)).

Te-doped and undoped InSb crystals were grown by the Czochralski method on earth (28). These crystals were remelted in space on board the Salyut-6 using the multipurpose apparatus Crystal. Part of the sample remained unmelted and served as a seed. In this way directional solidification of the melt was maintained. The structural perfection of the crystals grown in space was substantially superior to that of crystals grown on earth. The experimenters failed to obtain Te-doped InSb single crystals on earth. Generally all ingots had the structure of small blocks. These blocks did not retain the growth direction and on their crystal boundaries were often observed accomodation bands suggesting high stresses had been near the boundaries. Typical defects included shallow etch pits, dislocation nets decorated by impurity, microtwins, and large inclusions at the seed part of the crystals. Dislocation densities of these crystals were greater than $10^6/cm^2$. The crystals grown in space had large single blocks stretched along the growth direction given by the seed with a <211> orientation. Conjugation boundaries of the blocks were usually twin boundaries. The absence of dislocation arrays near the conjugation boundaries

indicated that they were coherent, i.e., during its growth the crystal didn't experience thermoelastic stresses. The dislocation densities did not exceed 2 x $10^5/cm^2$ and some blocks had densities as low as $10^3/cm^2$. Large inclusions were not found.

For the undoped InSb crystals grown on earth and in space, the following characteristics were observed. The earth-grown undoped InSb crystals exhibited a dislocation density greater than 5 x $10^3/cm^2$ near the seed end of the crystal. With crystal growth the dislocation density increased by two or more orders of magnitude and a cell dislocation structure was generated. Twin lamellae stretched along the ingot growth direction as well as accomodation bands. The dislocation density in the undoped crystal investigated both in the seed and the space-recrystallized regions was 2.5 x $10^1/cm^2$. This was considered to be an essentially dislocation-free crystal. This density remained constant along the length of the whole ingot. Unfortunately, growth conditions were such that a great number of growth twins were generated. The twinning occurred along the (111) plane at an angle of 71° to the <211> growth axis and it began at 2.5 mm from the seeding boundary. At the seed end of the ingot the distance between the twins was 2 mm, but as the ingot grew it reduced to 0.2 mm. Dislocation arrays were absent near the twins, thus it was concluded that coherent twinning took place. Kashimov (28) stated that the generation of twins is known to be connected with preliminary atom association, the extent of melt supercooling and the extent of chemical content deviation from stoichiometry. He attributed twin formation in this study to high supercooling and deviations from stoichiometry. The deviations from stoichiometry

were evident from the monotonic increase in the lattice parameter from the beginning to the end of the recrystallized region (28,29,30).

According to Antonov et al (31), the twin boundary energy in InSb is one-half the stacking fault energy. They propose that twins form mechanically as a stress relief during crystal growth or also that they form at the crystallization front by atomic packing errors. Statistical analyses were performed on the number of twins formed in zone melting and Czochralski growth. From this information the authors suggested that twin formation was probably due to packing fault errors. They also found that the frequency of twinning increased sharply with increases in supercooling, presumably caused by increasing growth rates. Again, these conclusions are premature. The cause and effect relationships of these situations have not been fully explored.

Many different methods of growing GaSb have been attempted, but the crystals usually contained macro- and microdefects such as twins and macrofacets (32, 33). A high quality GaSb bicrystal was grown in a Bridgman type apparatus under microgravity conditions on board of Salyut-6 (34,35). The space grown crystal exhibited good surface quality. There were ridges on the surface similar to those found in InSb during the Skylab program (12). The majority of these ridges were oriented. Part of them encompassed the ingot perpendicular to the growth direction and others made zigzags in different places, branching at angles which were odd multiples of 15^{o}. Several intergrowths of twin crystals were noted. Growth began on several

seed crystals and then decreased to two. Because interaction of the solidified material with the ampoule wall apparently was at a minimum, heat removal was thought to have occurred primarily along the axis. The authors believed that this condition led to a uniform defect distribution.

The earth-grown sample grown under the same conditions contained many more fine grained crystallites than the space sample. The extensive formation of crystallites and twins on the ingot periphery was attributed to the deforming effect of the ampoule. This effect was observed along the entire length of the ingot. In moving from the ingot surface to the middle, the dislocation density and the number of large angle grain boundaries increased.

Sen (16) performed an investigation of the effect of different paramaters on twin formation in dodecanedicarboxylic acid (DDA) during directional solidification in thin cells. Foreign particles increased twinning when the difference in the coefficient of thermal expansion was large. The number of twin boundaries increased slightly with growth rate, but decreased drastically with temperature gradient. Twin boundaries started at polycrystals formed at the growth interface and terminated upon meeting another twin or grain boundary. Zone refining significantly reduced twin formation. However, twin formation was restarted in zone refined DDA by adding soluble impurities with similar molecular structure and size.

IV. Spin-Up/Spin-Down

Spin-up/spin-down is the process of adjustment of an initially uniformly-rotating fluid of angular velocity w_o to an imposed change in the rotation rate of its container to w (38). It is a means of mixing a melt. This method has evolved in crystal growth, because direct agitation may be difficult. This may be due to corrosion concerns or because the ampoule may have to be sealed from the environment to prevent volatiles from escaping or reacting with the surrounding atmosphere. Spin-up/spin-down is also known as Accelerated Crucible Rotation Technique (ACRT) when referring to crystal growth.

Uniform crucible rotation does not lead to adequate mixing of a melt, because the crucible and the melt rotate at the same angular velocity, although it will tend to decrease temperature differences due to a thermally asymmetric furnace. Conversely, bringing a crucible from rest to rotation will bring about effective stirring of the liquid. Fluid near the crucible wall will follow any changes in the motion with little delay. Fluid which is closer to the interior will tend to continue its previous motion due to inertia. The resulting pattern of motion is one of slippage and shear around the rotation axis (39).

ACRT was applied to the Bridgman growth of incongruently melting Rb_2MnCl_4 from nonstoichiometric melts. The maximum growth rate of inclusion free crystals was increased by more than a factor of four over growth without spin-up/spin-down (40). Bridgman growth of

$Cd_xHg_{1-x}Te$ using ACRT resulted in a much greater degree of axial and radial homogeneity and an improvement in crystallinity (41,42,43). In the first documented application of ACRT, $GdAlO_3$ grew from a $PbO-PbF_2 - B_2O_3$ solution one thousand times larger than any previous attempts (44). ACRT has also been successfully applied to the Czochralski growth of silicon crystals (45).

Need to heat ampoule under vacuum to remove water, before putting in In, Ga, Sb.

CHAPTER 3

Experimental Procedure

take O_2-H_2 torch. Vycor might be easier okay.

Measured amounts of high purity (99.9999%) gallium, indium and antimony corresponding to one of three different compositions ($In_xGa_{1-x}Sb$, x =0.5, 0.3, 0.1) will be placed in a 9 mm ID and 11 mm OD fused silica ("quartz") tube. The tubes will be carbonized to prevent sticking of the melt and subsequent cracking of the ampoule during solidification. The silica tubes containing the elements will be evacuated to 5 to 10 Torr pressure and sealed to a total length of about 16 cm with a torch.

In clean system this is not necessary

Should back flush with 10% H_2 a few times to remove air + H_2O.

Sen (7) encountered some difficulty in introducing the desired amount of liquid gallium into the tube, because gallium in the liquid form readily sticks to fused silica. To overcome this, liquid gallium droplets of different sizes and weights were first placed on clean glossy weighing paper. They were then cooled slightly and solidified and were then much easier to handle. Formation of a thin layer of oxide on the gallium droplets could not be avoided in this process. Sen (7) found that this did not cause much of a problem, because after introducing the feed elements and evacuating, the gallium melted and a thin layer of oxide either came to the surface or adhered to the silica wall leaving clear gallium inside. Oxide formation was minimized when the gallium droplets were left in a dessicator prior to weighing and loading in the quartz ampoule. Sen

(7) also found that it was possible to remove oxide from the indium and antimony shot by placing them for 10 to 15 minutes in 1 HCl:2 H_2O (by volume) and then rinsing in methanol prior to weighing. This treatment produced clean and shiny shot.

must be well wiped first.

The contents of the ampoule will then be melted and directionally solidified in a Bridgman-Stockbarger apparatus. This apparatus consists of a heating section at the top and a cooling section at the bottom with a layer of insulation between the two. The layer of insulation ensures a more planar interface. To obtain a single crystal it is necessary to maintain the interface either planar or convex, which tends to prevent nuclei formed at the walls from growing inward. An ampoule containing the melt is translated from the heater into the cooler at a specific rate and the melt is solidified. The rate of solidification is equal to the translation rate except near the ends of the ampoule. The Bridgman-Stockbarger apparatus has the advantage of permitting independent control of interface shape, interfacial temperature gradient and growth rate.

show diagram

The ampoule will be placed inside the furnace. The voltage required to produce the desired heater temperature will be turned on along with the cold water circulator. The ampoule will be left stationary for 24 hours to permit temperature equlibrium and melt homogenization. The lowering operation will then be started at rates of up to 4 mm/day so that 20 days will be required to grow an ingot of 8 cm long. In the trials where spin-up/spin-down is to be employed, the ampoule will be rotated from rest for a period of a few seconds, stopped and then rotated in the other direction. After the

may not be long enough. Do with spin-up spin-down

Probably good idea to

growth period the heater power and cold water circulation will be turned off successively. When the heater cools down to room temperature, the ampoule will be taken from the furnace and placed in concentrated hydroflouric acid overnight so as to dissolve the ampoule. The entire ingot should be extracted clean and intact by this method.

& Be very careful with HF. Do in hood. Don't breathe it. Keep hands wet with H_2O periodically while using.

The ingots will then be cut longitudinally, sandblasted and then chemically etched to show contained microstructures more clearly. These will then be examined using polarized incident light for the number of grain and twin boundaries. A scanning electron microscope with an energy disspersive spectrometer will also be used to view the longitudinal and transverse sections of the alloy for radial and longitudinal homogeneity.

Remember that twin boundaries may appear curved in optical microscope. Need higher magnification of SEM to distinguish.

What sort of results do you expect?

How will you construct apparatus? (Parts list, vendors, etc.)

Where buy high purity In, Ga, Sb? Prices?

T[illegible] + sheets?

REFERENCES

1. T.S. Plaskett and J.F. Woods, J. Crystal Growth 11 (1971) 341-4.

2. A. Joullie, J. Allegre and G. Bougnot, Mat. Res. Bull. 7 (1972) 1101-1108.

3. E. Lendvay, M. Harsy, T. Gorog, I. Gyuro, I. Pozsgai, F. Koltai, G. Gyulai, T. Lohner, G. Mezey, E. Kotai, F. Paszti, V.T. Hrjapov, N.A. Kultchisky and L.L. Regel, J. Crystal Growth 71 (1985) 538-550.

4. V.I. Ivanov-Omskii and B.T. Kolomiets, Soviet Phys. Solid State 1 (1959) 834.

5. W.A. Tiller, K.A. Jackson, J.W. Rutter and B. Chalmers, Acta Met. 1 (1953) 428.

6. W.W. Mullins and R.F. Sekerka, J. Appl. Phys. 34 (1963) 323.

7. S. Sen, Ph.D. Thesis, University of Southern California (1975).

8. J. Yee, W.R. Wilcox, K. Sarma and S. Sen, Skylab Report (1974).

9. R. Kern, Bull. Soc. Franc. Mineral Cristallogr. 84 (1961) 292.

10. G. Friedel, Lecons de Cristallographie, Paris: Berger-Levrault (1926); "through R.W. Cahn, Adv. Physics A Quart. Suppl. Phil. Mag. 3 (1954) 1."

11. R.W. Cahn, Advances in Physics A Quart. Suppl. of the Phil. Mag. 3 12 (1954) 1.

12. A.F. Witt, H.C. Gatos, M. Lichtensteiger, M. Lavine and C.J. Herman, "Proc. of Third Space Processing Symposium, Skylab Results", NASA Technical Report M-74-5 1 (1977).

13. H. Gleiter, Acta Met. 7 (1969) 1421.

14. K.A. Jackson, Acta Met. 3 (1965) 1212.

15. E. Billig, J. Inst. Metals 83 (1954-55) 53.

16. R. Sen, Ph.D. Thesis, Clarkson University (1985).

17. R.S. Wagner and H. Brown, Trans. Met. Soc. AIME. 224 (1962) 1185.

18. P. Hartman, Z. Kristallogr. 107 (1956) 225-237.

19. J.F. Yee, M.C. Lin, K. Sarma, W.R. Wilcox, J. Crystal Growth 30 (1975) 185-192.

20. R.A. Lefever, W.R. Wilcox, K. Sarma, Mat. Res. Bull. 13 (1978) 1175-80.

21. J.F. Yee, S. Sen, K. Sarma, M.C. Lin, W.R. Wilcox, "Proc. of 3rd Space Processing Symp., Skylab Results", 1 (1977) 301.

22. K. Sarma, Ph.D. Thesis, University of Southern California (1976).

23. S. Sen, W.R. Wilcox, and R. A. Lefever, Met. Trans. A, 9A March (1978) 462-4.

24. J.C. Woolley, J.A. Evans and C.M. Gillett, Proc. Phys. Soc. London 74 (1959) 244.

25. W.M. Coderre and J.C. Woolley, Can. J. Phys. 46 (1968) 1207.

26. A.F. Witt, H.C. Gatos, M. Lichtensteiger, M.C. Lavine, and J.C.Herman, J. Electrochem. Soc. 122 (1975) 276-283.

27. H.U. Walter, J. Electrochem. Soc. 124 (1977) 250-258.

28. F.R. Kashimov et al., Proc. 3rd European Symp. Material Sciences in Space, Grenoble, 24-27 April 1979 - ESA SP-142 (June 1979) p. 9-15.

29. E.A. Dem'yanov, Soviet Physics-Crystallography 15 (1971) 690.

30. E.A. Dem'yanov, V.V. Smirnov, and S.A. Stroitelev, Inorganic Materials 4 (1968) 1591.

31. P.I. Antonov, S.I. Bakholdin, Yu G. Nosovand, E.S. Kalitina,

Akad. Nauk USSR, Physics (Bull. Akad. Sci. USSR, Physical Series) 47 (1983) 101.

32. Yu.A. Osip'yan and L.L. Regel', Editors, Salyut-6-Soyuz, Material Sciences and Technology, (USSR, Academy of Sciences, Space Research Institute) Nauka Press, Moscow, (1985) 1-177.

33. E. Lendvay, M. Harsy, T. Gorog, I. Gyuro, I.Pozsgai, F.Koltai, J. Gyulai, T.Lohner, G. Mezey, E. Kotai, F. Paszti, V.T. Hrjapov, N.A. Kultchisky and L.L. Regel, J. Crystal Growth 71 (1985) 538.

34. M. Kumagawa, J. Crystal Growth 44 (1978) 291.

35. M. Kumagawa and N.V. Quang, Jap. J. Appl. Phys. 19 (1980) 2509.

36. N.V. Quang, Y. Nayakawa and M. Kumagawa, Jap. J. Appl. Phys. 20 (1981) 329.

37. G.B. Blom and T.S. Plaskett, J. Electochem. Soc. 118 (1971) 1831.

38. H.P. Greenspan, "The Theory of Rotating Fluids," Cambridge University Press, London, U.K. (1968).

39. H.J. Scheel and E.O. Schulz-DuBois, J. Crystal Growth 12 (1972) 81.

40. A. Horowitz, D. Gazit, J. Makovsky and L. Ben-Dor, J. Crystal Growth 61 (1983) 323.

41. P. Capper, C.L. Jones, E.J. Pearce and M.J.T. Quelch, J. Crystal Growth 62 (1983) 487.

42. J.J. Gosney, P. Capper, C.L. Jones and I. Kenworthy, Private Communication, Clarkson University 1984.

43. P. Capper, J.J.G. Gosney and C.L. Jones, J. Crystal Growth 70 (1984) 356.

44. H.J. Scheel, E.O. Schulz-DuBois, J. Crystal Growth 8 (1971) 304.

45. W.J. Patrick and W.A. Westdrop, U.S. Patent 4,040,895 (9 August 1977).